Supplementary Information (SI) for Chemical Science.

Supporting Information

Polyoxometalate Condensation and Transformation Mediated by Adaptive Coordination-Assembled Molecular Flasks

Li-Xuan Cai,[a, c] Yu-Hang Hu,[a, b] Li-Peng Zhou,[a, c] Pei-Ming Cheng,[a] Xiao-Qing Guo,[a] Yi-Tsu Chan,[d] Qing-Fu Sun*[a, c]

[a] State Key Laboratory of Structural Chemistry, Fujian Institute of Research on the Structure of Matter, Chinese Academy of Sciences, Fuzhou 350002, PR China

[b] College of Chemistry and Materials Science, Fujian Normal University, Fuzhou, 350007, PR China

[c] University of Chinese Academy of Sciences, Beijing 100049, PR China

[d] Department of Chemistry, National Taiwan University, Taipei 10617, Taiwan

Contents

1. General

Unless otherwise noted, all chemicals and solvents were purchased from commercial sources and used without further purification. Deuterated solvents were purchased from Adamas-Beta, Sigma-Aldrich and J&K scientific. 1D and 2D NMR spectra were measured by using a Bruker BioSpin AVANCE III 400, JNM-ECZ600R/S1 spectrometer or JEOL JNM-ECZ400S/L1 NMR spectrometer. The NMR chemical shifts (δ) are reported in ppm (parts per million) and were determined with respect to solvent signal originated due to incomplete deuteration of the solvents ($\delta = 4.79$ for D_2O, $\delta = 2.50$ for DMSO-d_6 in ^1H NMR). The FT-IR (KBr pellet) spectra were recorded on an ABB Bomem MB102 IR spectrometer. Electro-spray-ionization time-of-flight mass-spectroscopy (ESI-TOF-MS) were recorded on an Impact II UHR-TOF mass spectrometry from Bruker with tuning mix as the internal standard, or other mass spectrometers as specified below. Data analysis was conducted with the Bruker Data Analysis software (Version 4.3) and simulations were performed with the Bruker Isotope Pattern software. Synthesis of cage **1** was following the previous reported procedures.[S1]

2. Synthesis of Mo-based host-guest complexes.

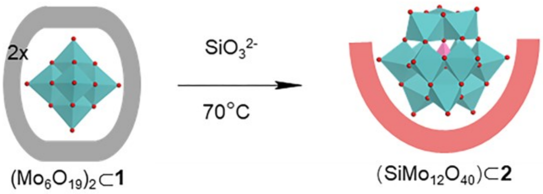

Scheme S1. Synthesis of host-guest complex $(SiMo_{12}O_{40})\subset\mathbf{2}\cdot(NO_3)_8$.

$(Mo_6O_{19})_2\subset\mathbf{1}\cdot(NO_3)_8$ was synthesized according to a similar procedure of our previous work.[S2] 2 Equiv. of $(TBA)_2Mo_6O_{19}$ (120 uL, CH_3CN) was added into the solution of cage **1** $\cdot(NO_3)_{12}$ in H_2O (0.5 mL, 2 mM) with stirring for 30 min. After removing the solvent and redissolving in D_2O (0.5 mL) in a NMR tube, 1 equiv. of Na_2SiO_3 was added into the resulting solution, followed by heating at 70°C for 12 hours. ^1H NMR evidenced the complete formation of the host-guest complex $(SiMo_{12}O_{40})\subset\mathbf{2}\cdot(NO_3)_8$. NMR spectra are available below. ^1H NMR for $(Mo_6O_{19})_2\subset\mathbf{1}\cdot(NO_3)_8$ (400 MHz, D_2O) δ 9.22 (d, $J = 6.0$ Hz, 9H), 9.15 (d, $J = 6.4$ Hz, 9H), 9.02 (d, $J = 5.6$ Hz, 8H), 8.96 (d, $J = 6.4$ Hz, 8H), 8.92 (d, $J = 6.0$ Hz, 8H), 8.64 (d, $J = 5.6$ Hz, 8H), 7.69 (s, 8H), 5.86 (s, 8H), 3.08 (s, 16H), 2.65 (d, $J = 11.6$ Hz, 48H). Diffusion coefficient (D_2O, 298 K): $D = 2.43\times10^{-10}$ m^2s^{-1}. ^1H NMR (400 MHz, D_2O) δ 9.31 (d, $J = 8.0$ Hz, 8H), 9.25 (d, $J = 6.0$ Hz, 4H), 9.17 (d, $J = 6.0$ Hz, 4H), 9.04 (d, $J = 6.8$ Hz, 8H), 8.78 (d, $J = 6.0$ Hz, 5H), 8.73 (dd, $J_1 = J_2 = 6.0$ Hz, 8H), 8.64 (d, $J = 6.8$ Hz, 7H), 8.37 (d, $J =6.0$ Hz, 4H), 7.53 (s, 8H), 5.91 (d, $J = 14.4$ Hz, 4H), 5.84 (d, $J = 14.4$ Hz, 4H), 3.08 (s, 24H), 2.88 (s, 8H), 2.80 (s, 8H), 2.67 (d, $J = 5.0$ Hz, 24H). Diffusion coefficient (D_2O, 298 K): $D = 1.75\times10^{-10}$ m^2s^{-1}. ESI-TOF-MS: m/z Calcd for $[2\cdot(SiMo_{12}O_{40}^{4-})]^{8+}$ 520.9199 found 520.9201.

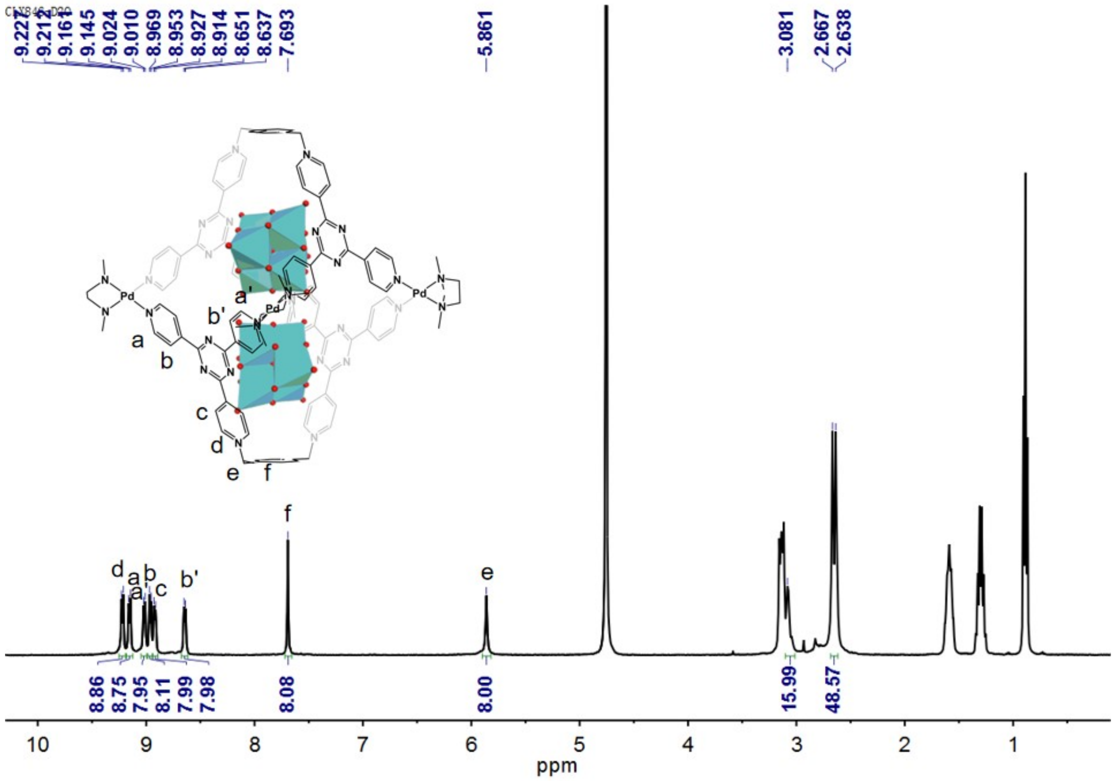

Figure S1. ^{1}H NMR spectrum of $(Mo_6O_{19})_2\subset\mathbf{1}\cdot(NO_3)_8$ (400 MHz, D_2O, 298 K).

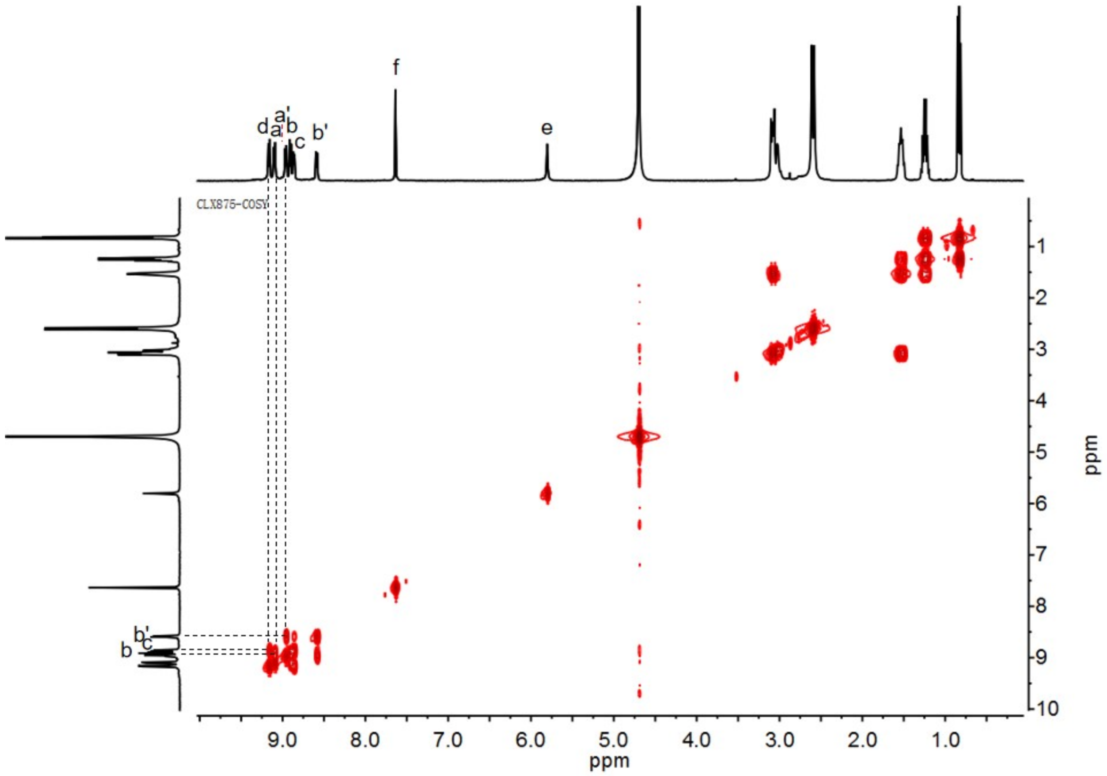

Figure S2. COSY NMR spectrum of $(Mo_6O_{19})_2\subset\mathbf{1}\cdot(NO_3)_8$ (400 MHz, D_2O, 298 K).

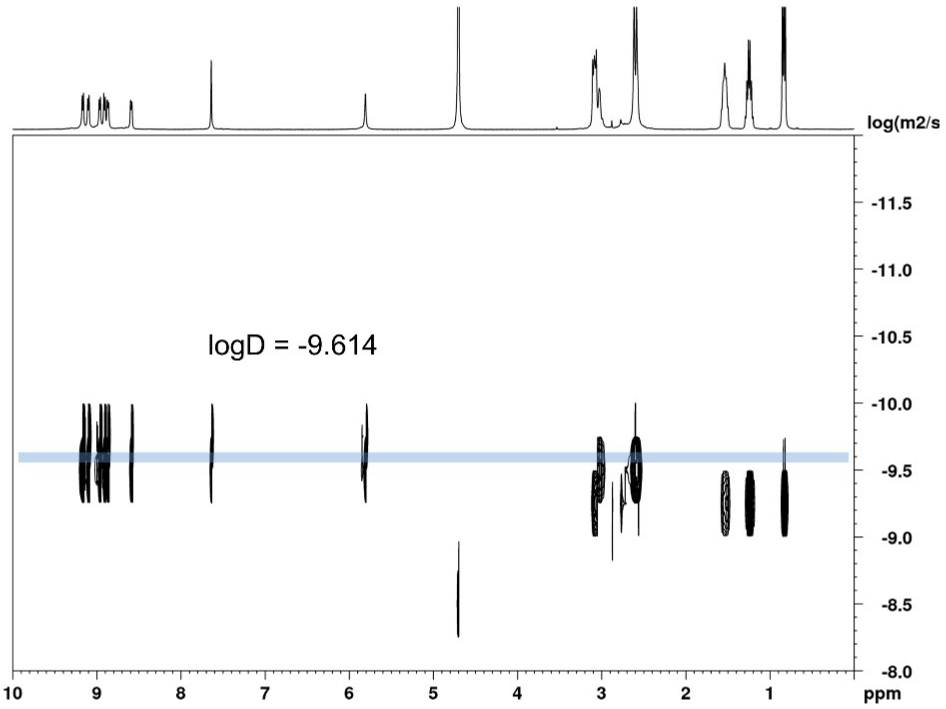

Figure S3. ^1H DOSY spectrum of $(Mo_6O_{19})_2\subset\mathbf{1}\cdot(NO_3)_8$ (400 MHz, D_2O, 298 K). Diffusion coefficient: $D = 2.43\times10^{-10}\ m^2s^{-1}$.

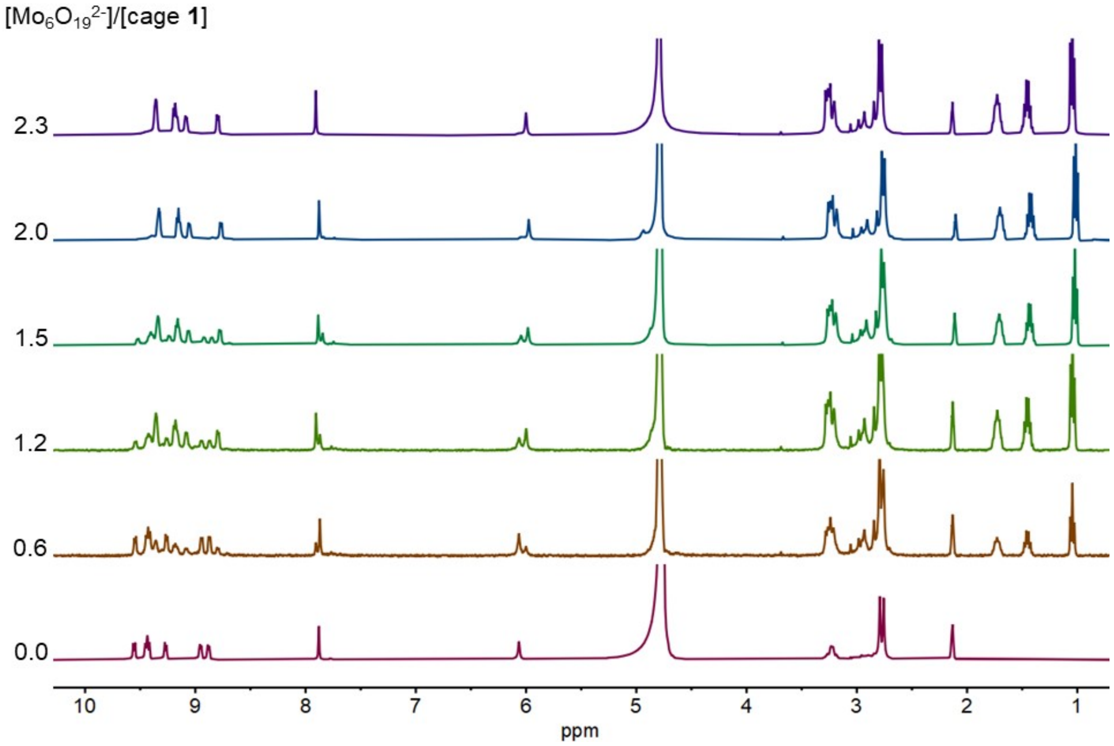

Figure S4. ^1H NMR titration spectra of cage $\mathbf{1}\cdot(NO_3)_{12}$ (1 mM) with 0 - 3 equiv. of $(TBA)_2Mo_6O_{19}$ (400 MHz, D_2O/CD_3CN 4/1, 298 K).

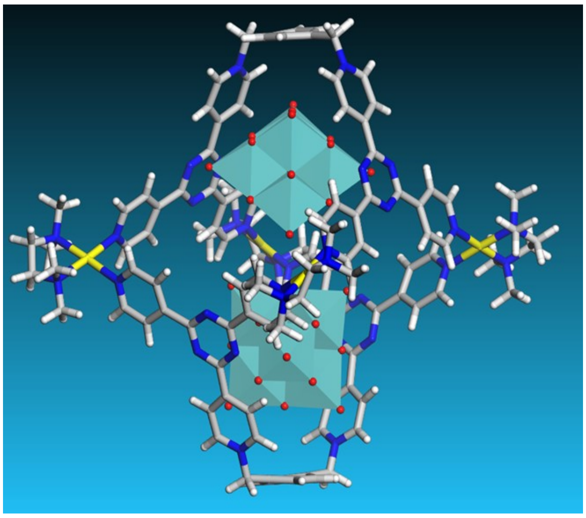

Figure S5. The MM modelled structures for $(Mo_6O_{19})_2\subset\mathbf{1}\cdot(NO_3)_8$ (Pd centers, yellow; C, gray; N, blue; H, white;). The $Mo_6O_{19}^{2-}$ anions are depicted in the polyhedra representation.

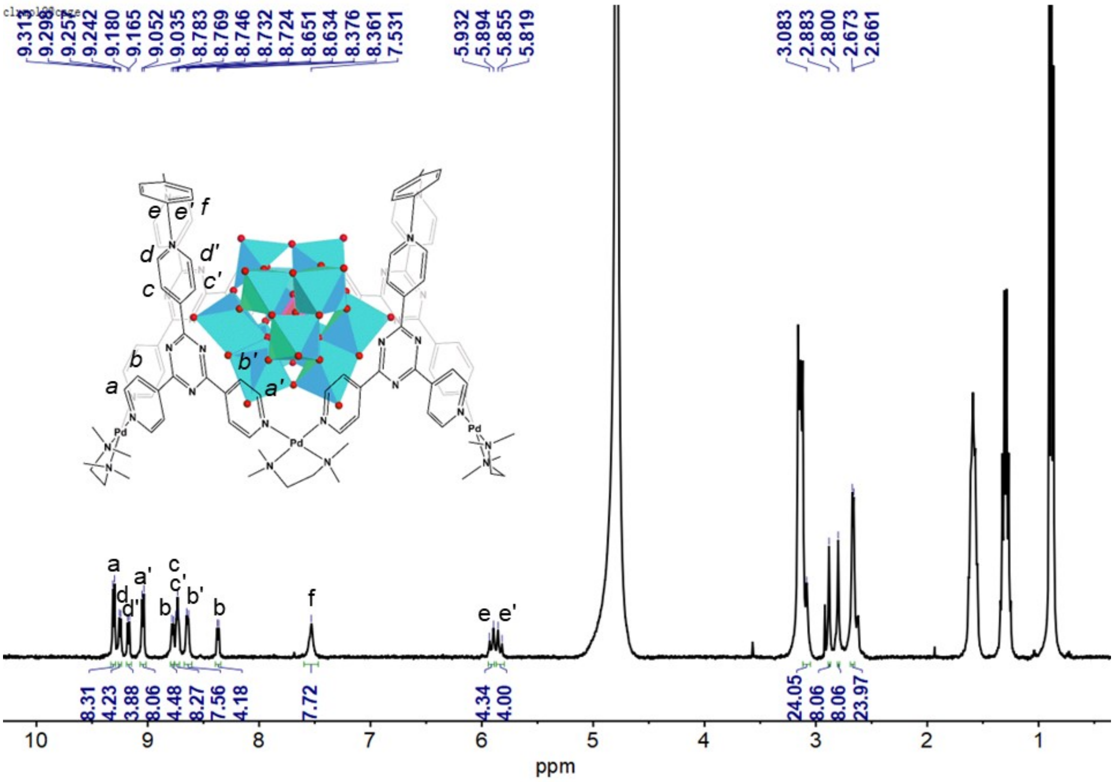

Figure S6. ${}^1H$ NMR spectrum of $(SiMo_{12}O_{40})\subset\mathbf{2}\cdot(NO_3)_8$ (400 MHz, D_2O, 298 K).

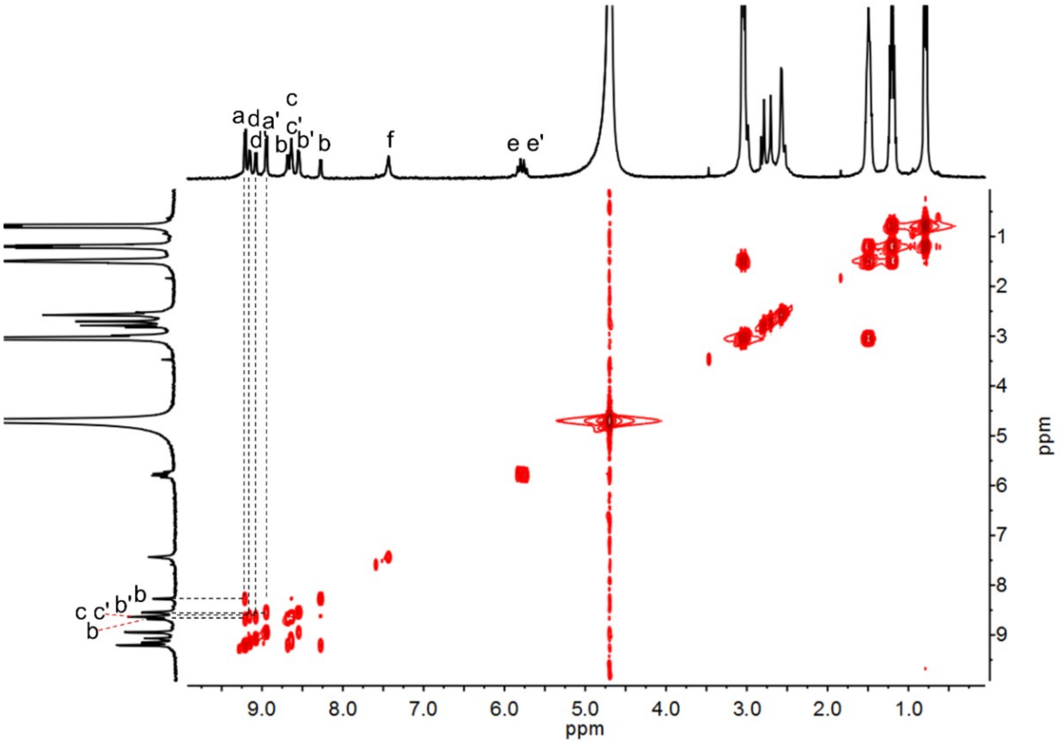

Figure S7. COSY NMR spectrum of $(SiMo_{12}O_{40})\subset\mathbf{2}\cdot(NO_3)_8$ (400 MHz, D_2O, 298 K).

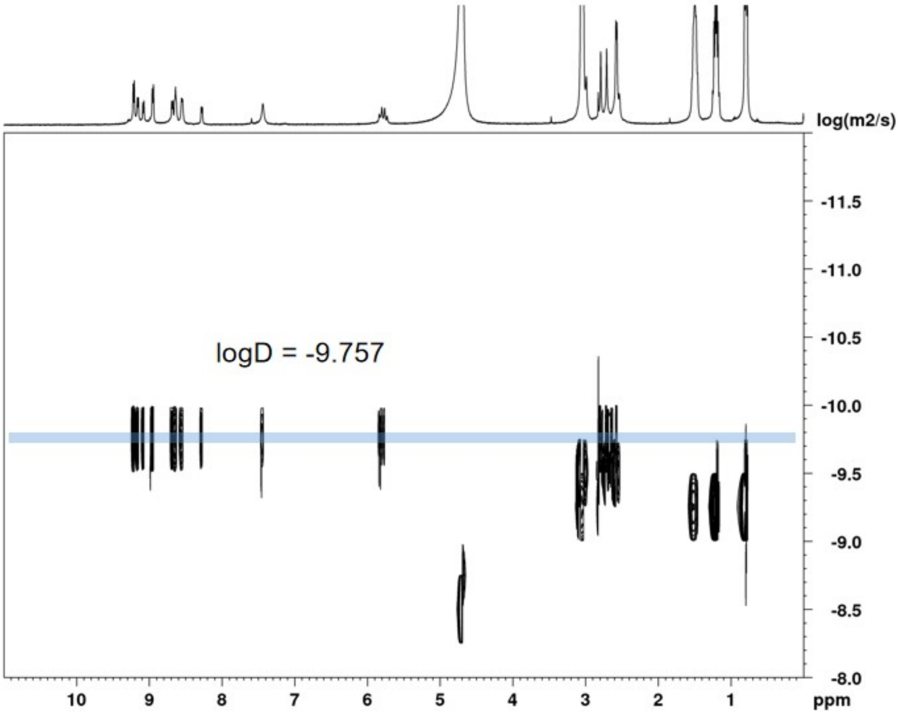

Figure S8. ^1H DOSY spectrum of $(SiMo_{12}O_{40})\subset\mathbf{2}\cdot(NO_3)_8$ (400 MHz, D_2O, 298 K). Diffusion coefficient: $D = 1.75\times10^{-10}\ m^2s^{-1}$.

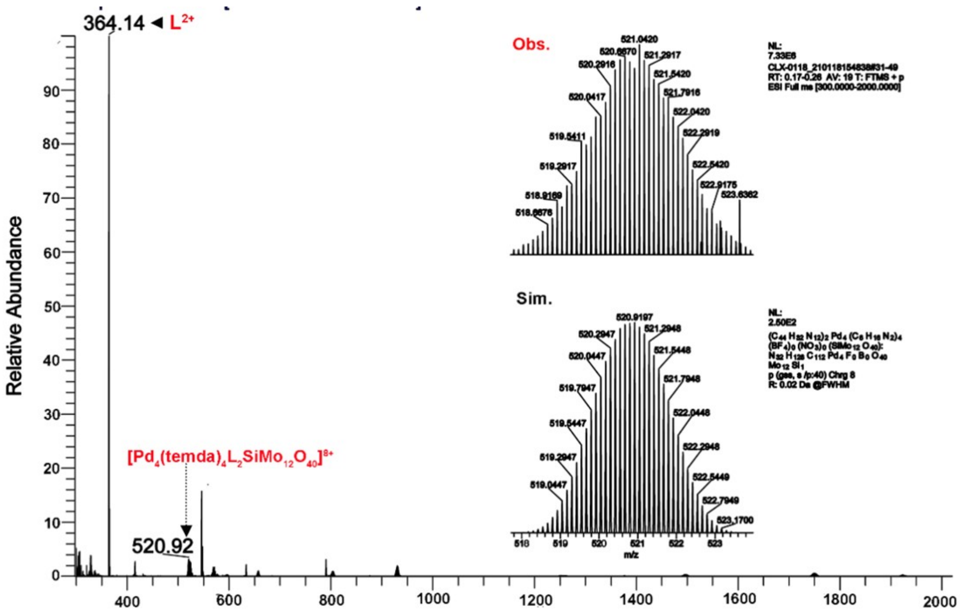

Figure S9. ESI-TOF-Mass spectrum (measured on an Exactive Plus mass spectrometry from Thermo Fisher Scientific) of $(SiMo_{12}O_{40})\subset\mathbf{2}\cdot(NO_3)_8$. The simulated and observed isotopic distributions of the 8+ peaks are well matched.

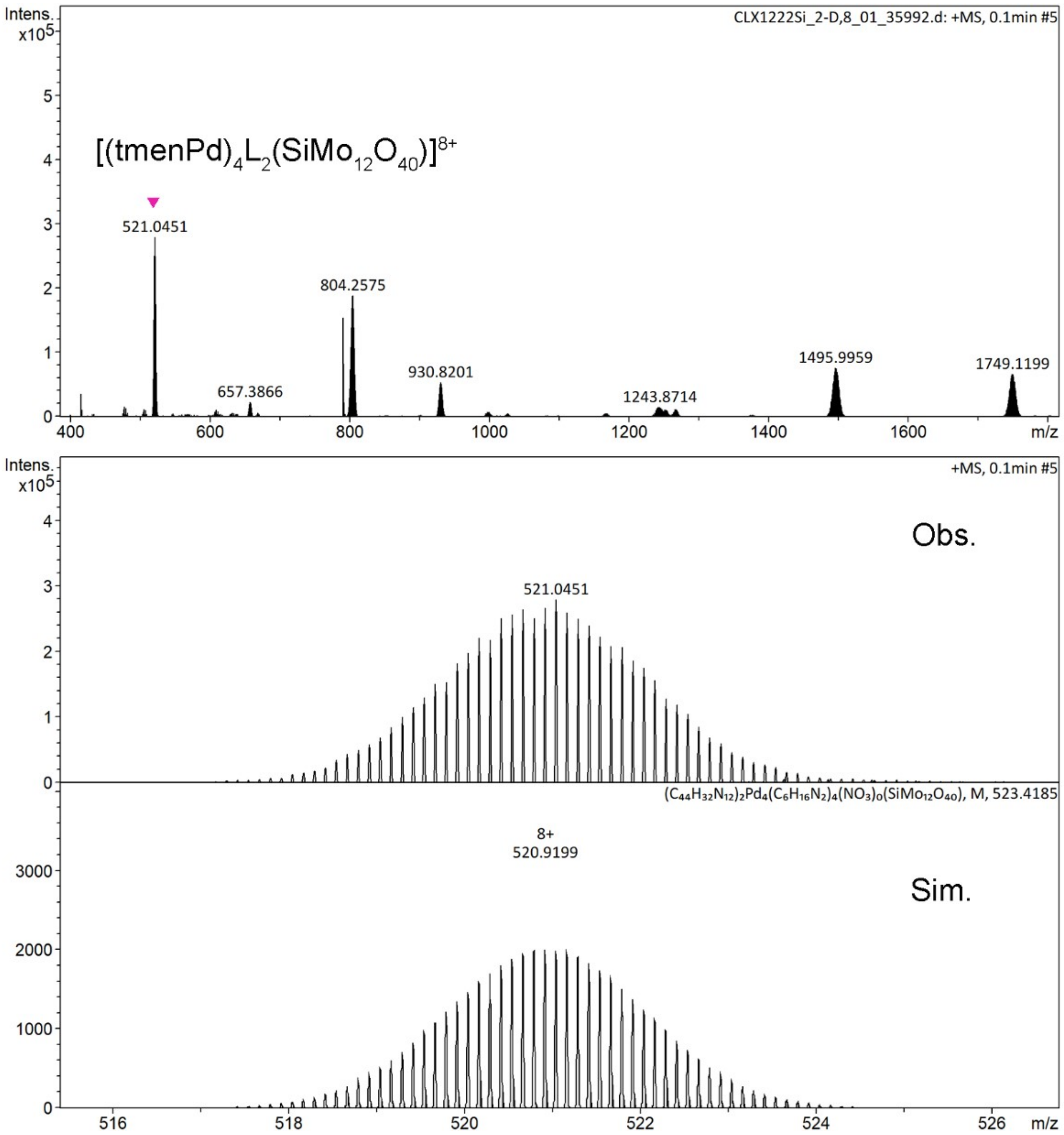

Figure S10. ESI-TOF-Mass spectrum (measured on an Impact II UHR-TOF mass spectrometry from Bruker) of $(SiMo_{12}O_{40})\subset\mathbf{2}\cdot(NO_3)_8$. The simulated and observed isotopic distributions of the 8+ peaks are well matched.

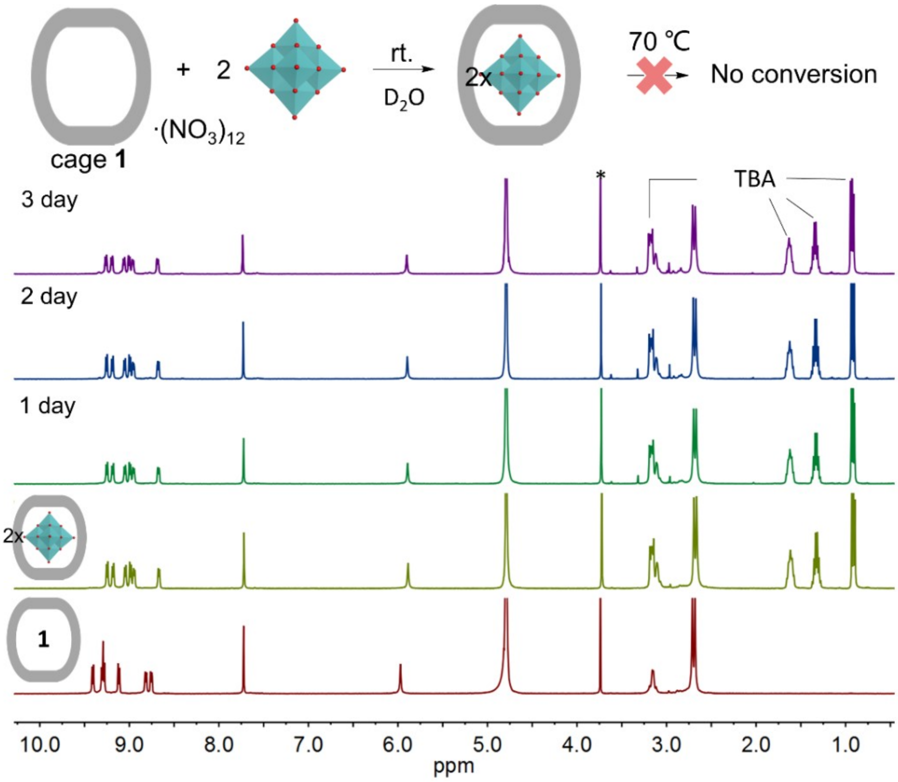

Figure S11. ^1H NMR change of $(Mo_6O_{19})_2$⊂**1**·$(NO_3)_8$ with heating time at 70°C (400 M, D_2O, 298 K). The signals marked * denote 1,4-dioxane as the internal standard.

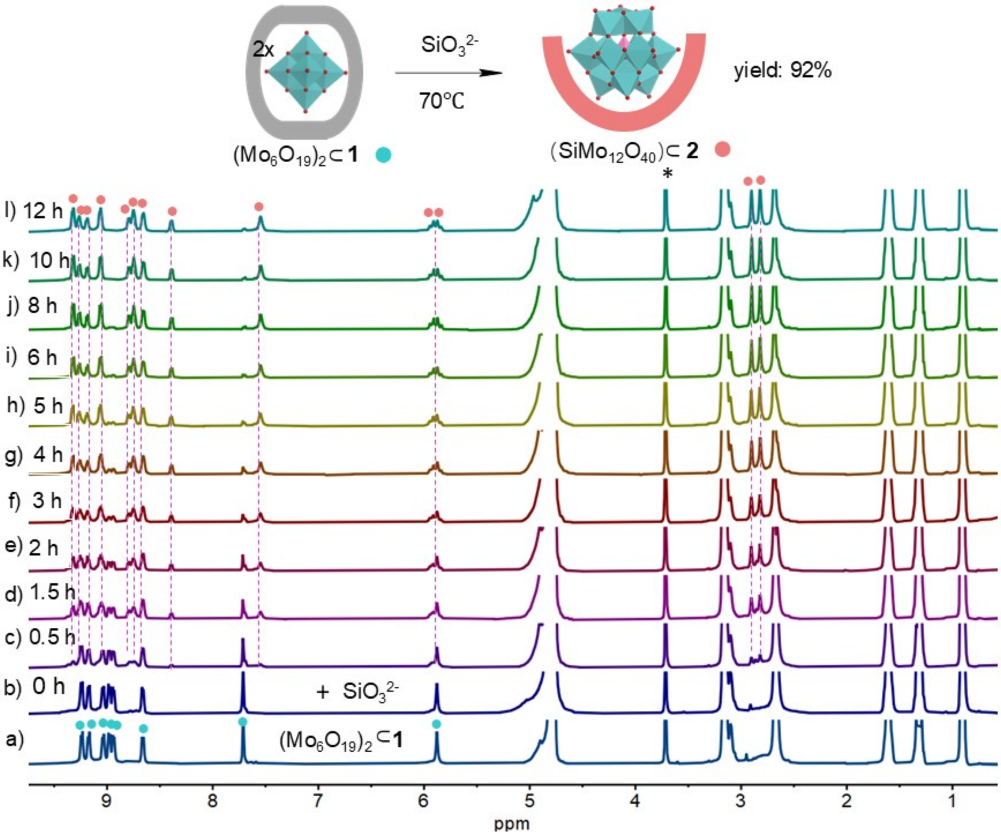

Figure S12. ^1H NMR change of $(Mo_6O_{19})_2$⊂**1**·$(NO_3)_8$ after adding 1 equiv. of Na_2SiO_3 and heated at 70°C (400 M, D_2O, 298 K). The signals marked * denote 1,4-dioxane as the internal standard.

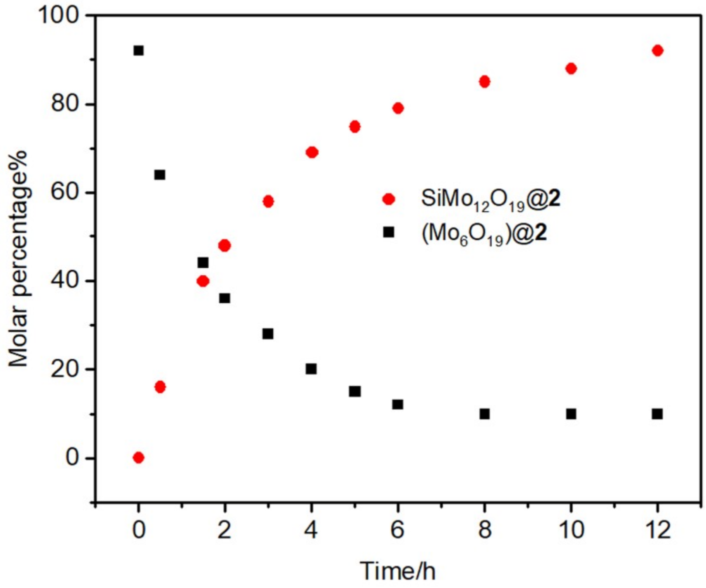

Figure S13. Molar percentage for the transformation reaction of $Mo_6O_{19}^{2-}$ (2 equiv.) and Na_2SiO_3 (1 equiv.) heating at 70°C in the presence of **1**·$(NO_3)_{12}$.

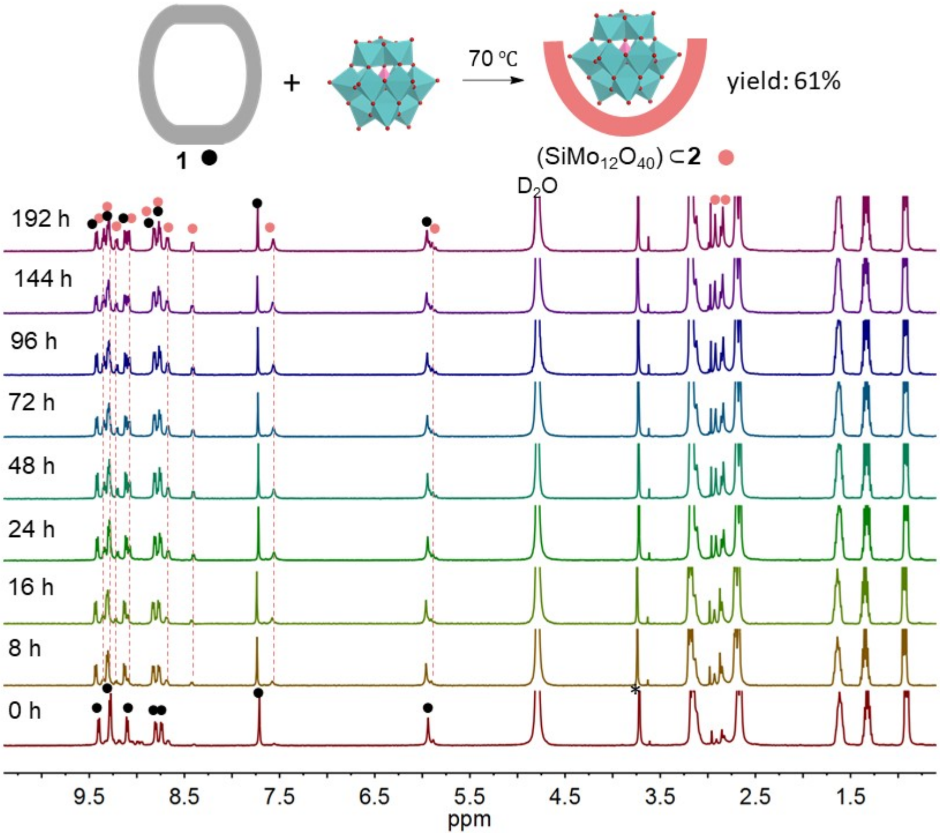

Figure S14. ^{1}H NMR change of cage **1**·$(NO_3)_{12}$ when adding 1 equiv. of $SiMo_{12}O_{40}^{4-}$ heated at 70°C.

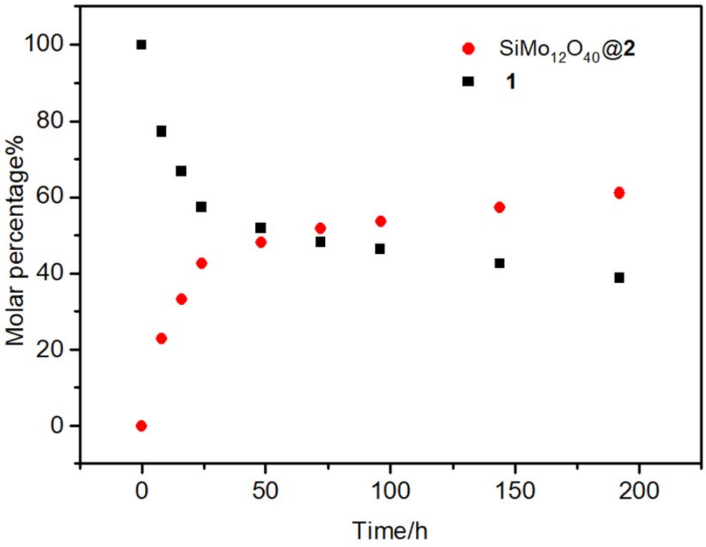

Figure S15. Molar percentage for the $SiMo_{12}O_{40}^{4-}$ induced structural transformation from **1** to **2** heated at 70°C.

3. Synthesis of W-based host-guest complexes.

2 Equiv. of $(TBA)_2W_6O_{19}$ (120 uL, CH_3CN) was added into the solution of cage **1**·$(NO_3)_{12}$ in H_2O (0.5 mL, 2 mM) with stirring for 30 min. Then the solution was heated at 70°C for a periour of time in the presence or without Na_2SiO_3. ^{1}H NMR evidenced the formation of the host-guest complex. ^{1}H NMR (400 MHz, D_2O) for $(W_6O_{19})\subset$**1**: δ 9.55 (d, *J* = 6.0 Hz, 8H), 9.43 (d, *J* = 6.4 Hz, 8H), 9.39 (d, *J* = 6.0 Hz, 8H), 9.30 (d, *J* = 6.4 Hz, 8H), 9.04 (d, *J* = 6.0 Hz, 8H), 8.94 (d, *J* = 6.0 Hz, 8H), 7.88 (s, 8H), 6.10 (s, 8H), 3.24 (m, 16H), 2.82 (s, 24H), 2.80 (s, 24H). Diffusion coefficient (D_2O, 298 K): D = 2.43×10^{-10} m^2s^{-1}.

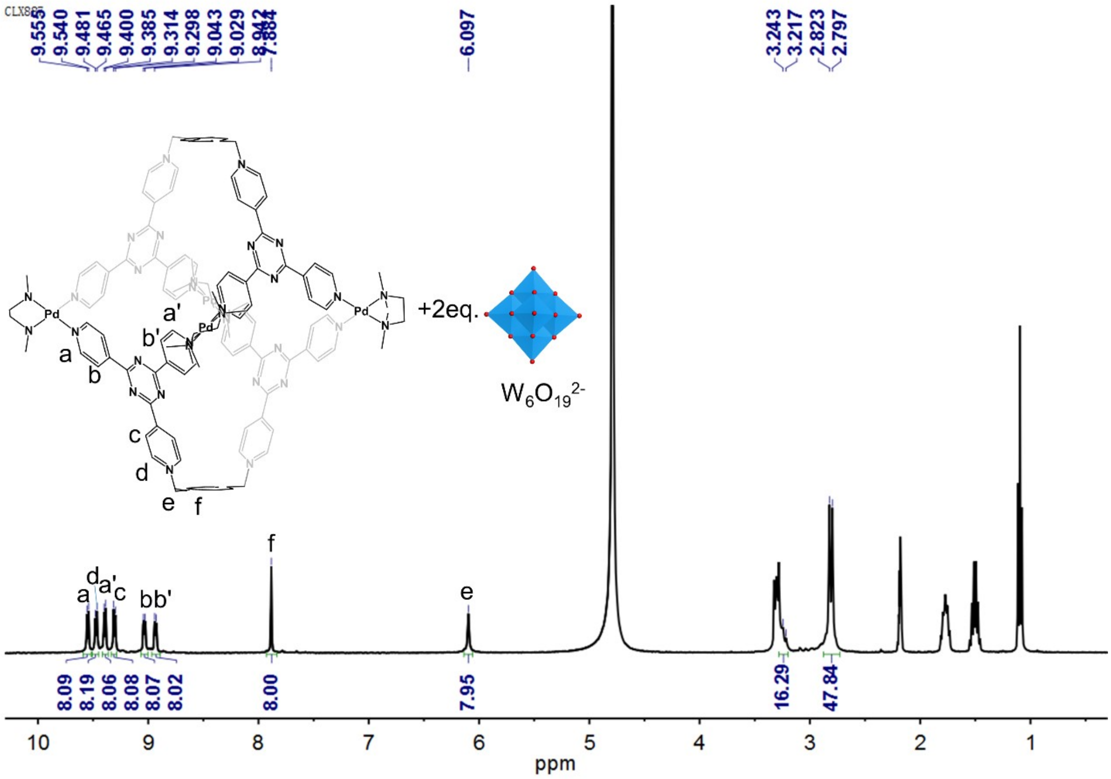

Figure S16. ^{1}H NMR spectrum of $(W_6O_{19})\subset$**1**$\cdot(NO_3)_{10}$ (400 MHz, D_2O, 298 K).

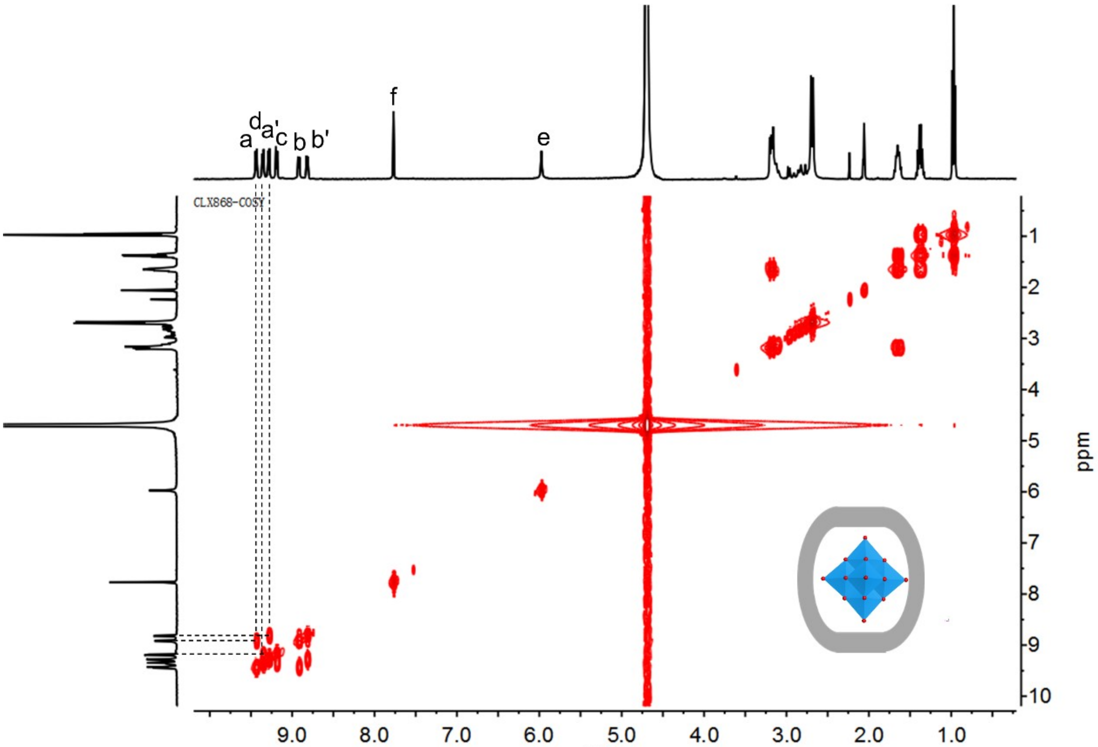

Figure S17. COSY NMR spectrum of $(W_6O_{19})\subset$**1**$\cdot(NO_3)_{10}$ (400 MHz, D_2O, 298 K).

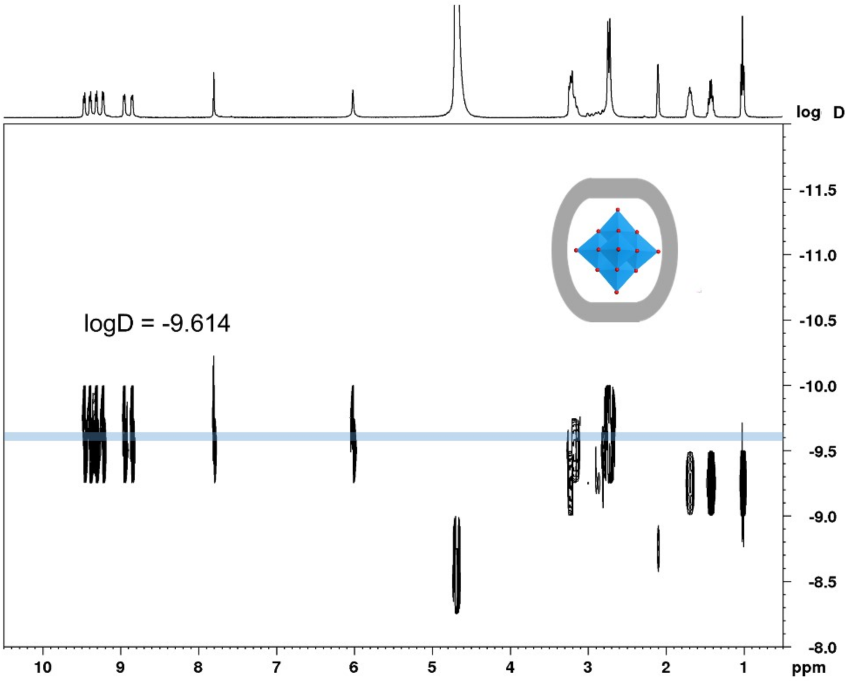

Figure S18. ^{1}H DOSY spectrum of $(W_6O_{19})\subset\mathbf{1}\cdot(NO_3)_{10}$ (400 MHz, D_2O, 298 K).

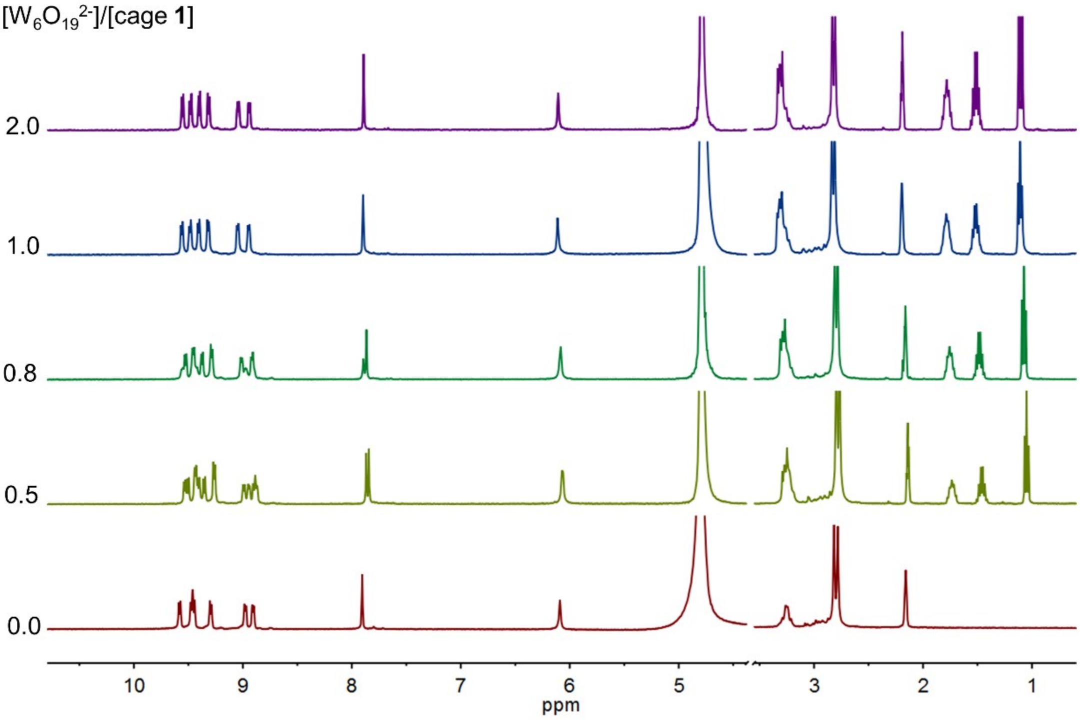

Figure S19. ^{1}H NMR spectra of a 1 mM solution of $\mathbf{1}\cdot(NO_3)_{12}$ in D_2O/CD_3CN (4/1) with 0-2.0 equiv. of $W_6O_{19}^{2-}$ anion.

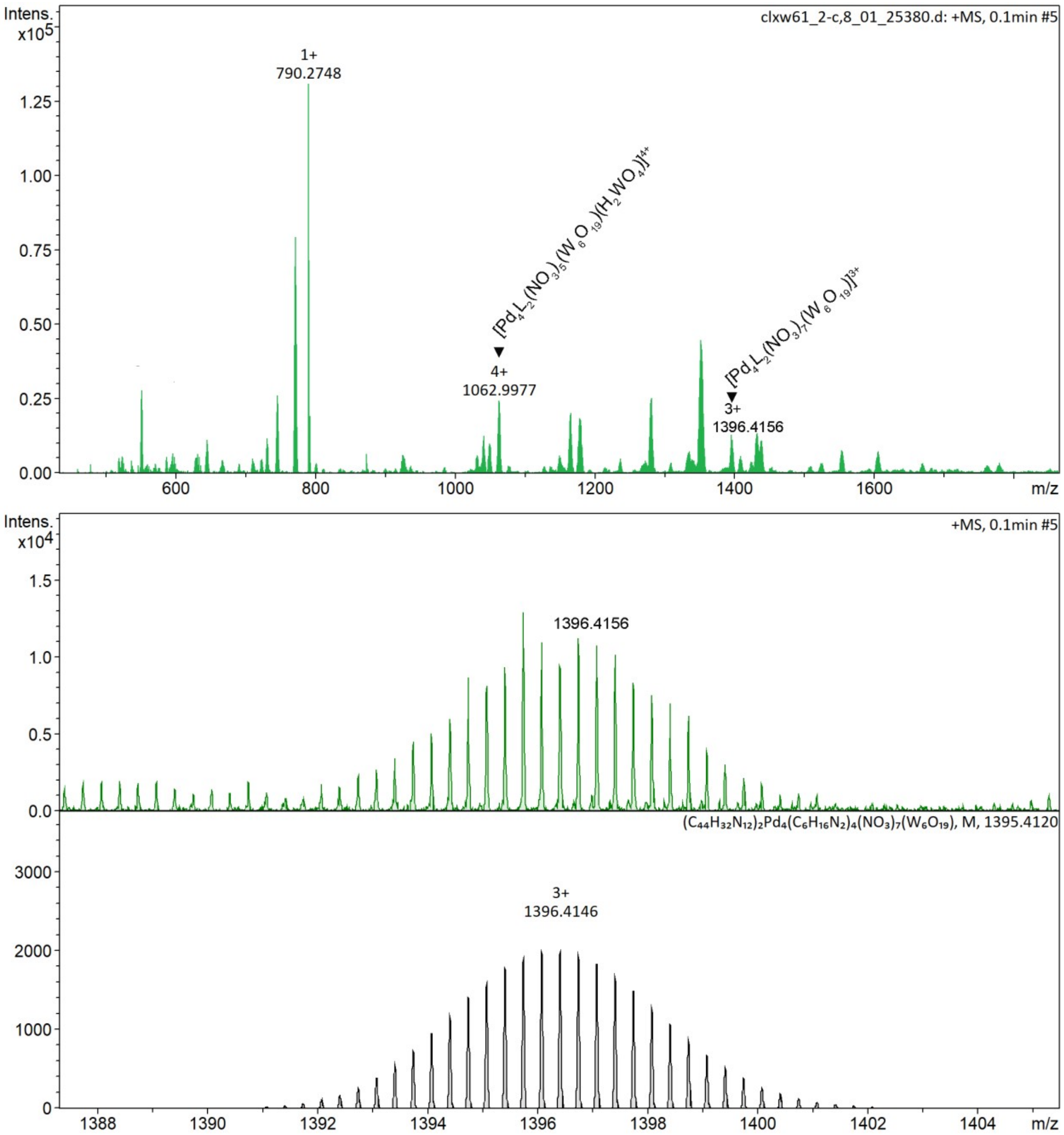

Figure S20. ESI-TOF-MS (measured on an Impact II UHR-TOF mass spectrometry from Bruker) of **1**·$(NO_3)_{12}$ with 2.0 equiv of $W_6O_{19}^{2-}$ anion. The simulated and observed isotopic distributions of the 3+ peaks corresponding to $[Pd_4L_2(NO_3)_7(W_6O_{19})]^{3+}$are well matched.

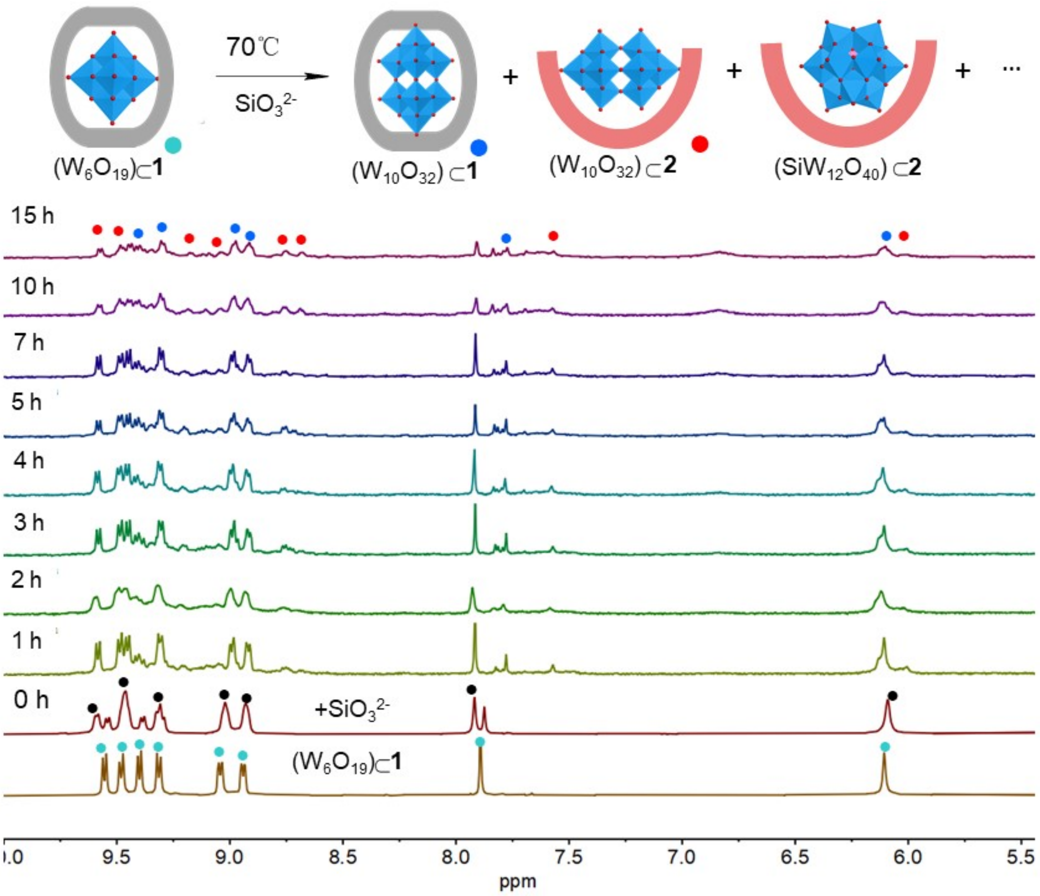

Figure S21. ^{1}H NMR change (400 M, D_2O/CD_3CN 4/1, 298 K) of $\mathbf{1}\cdot(NO_3)_{12}$ and 2 equiv. of $W_6O_{19}^{2-}$ with heating at 70°C upon addition of SiO_3^{2-}. The yields of the products $(W_{10}O_{32})\subset\mathbf{1}\cdot(NO_3)_8$ and $(W_{10}O_{32})\subset\mathbf{2}\cdot(NO_3)_8$ were calculated to be approximately 35% and 16%, respectively, using 1,4-dioxane as internal standard.

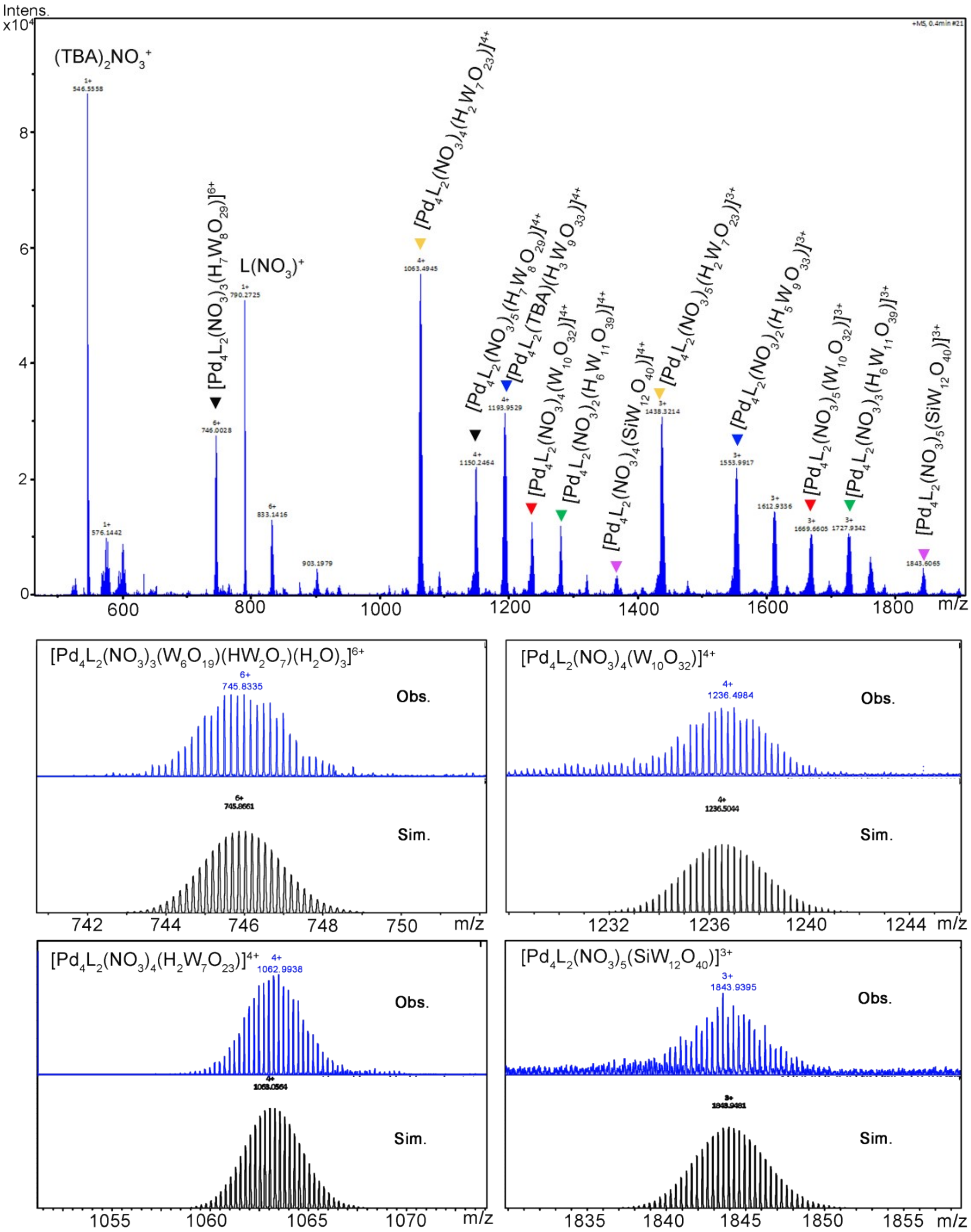

Figure S22. ESI-TOF-MS spectrum of **1**·(NO$_3$)$_{12}$ and 2 equiv. of W$_6$O$_{19}^{2-}$ after adding SiO$_3^{2-}$ and heating at 70°C for 2 days.

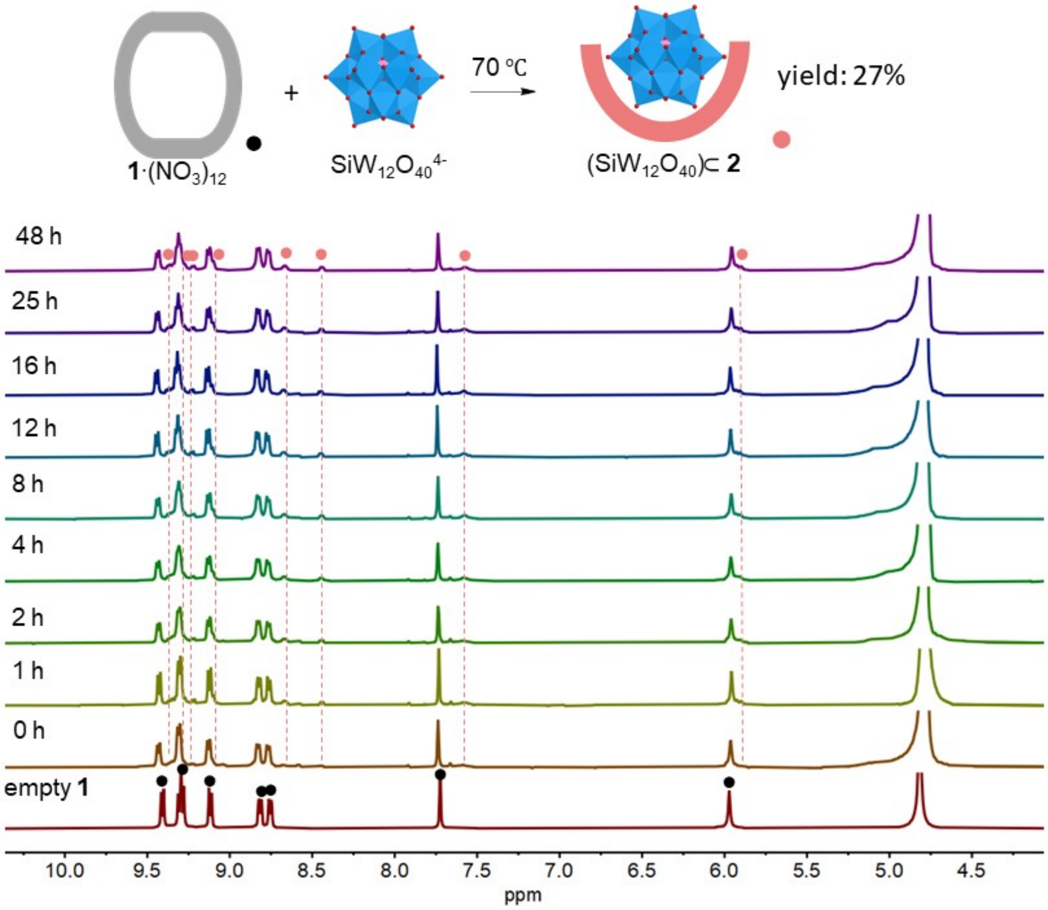

Figure S23. ^{1}H NMR change of $\mathbf{1}\cdot(NO_3)_{12}$ and 1 equiv. of $SiW_{12}O_{40}^{4-}$ with heating time at 70°C (400 M, D_2O, 298 K). The yield of $(SiW_{12}O_{40})\subset\mathbf{2}\cdot(NO_3)_8$ were calculated to be approximately 27% using 1,4-dioxane as internal standard.

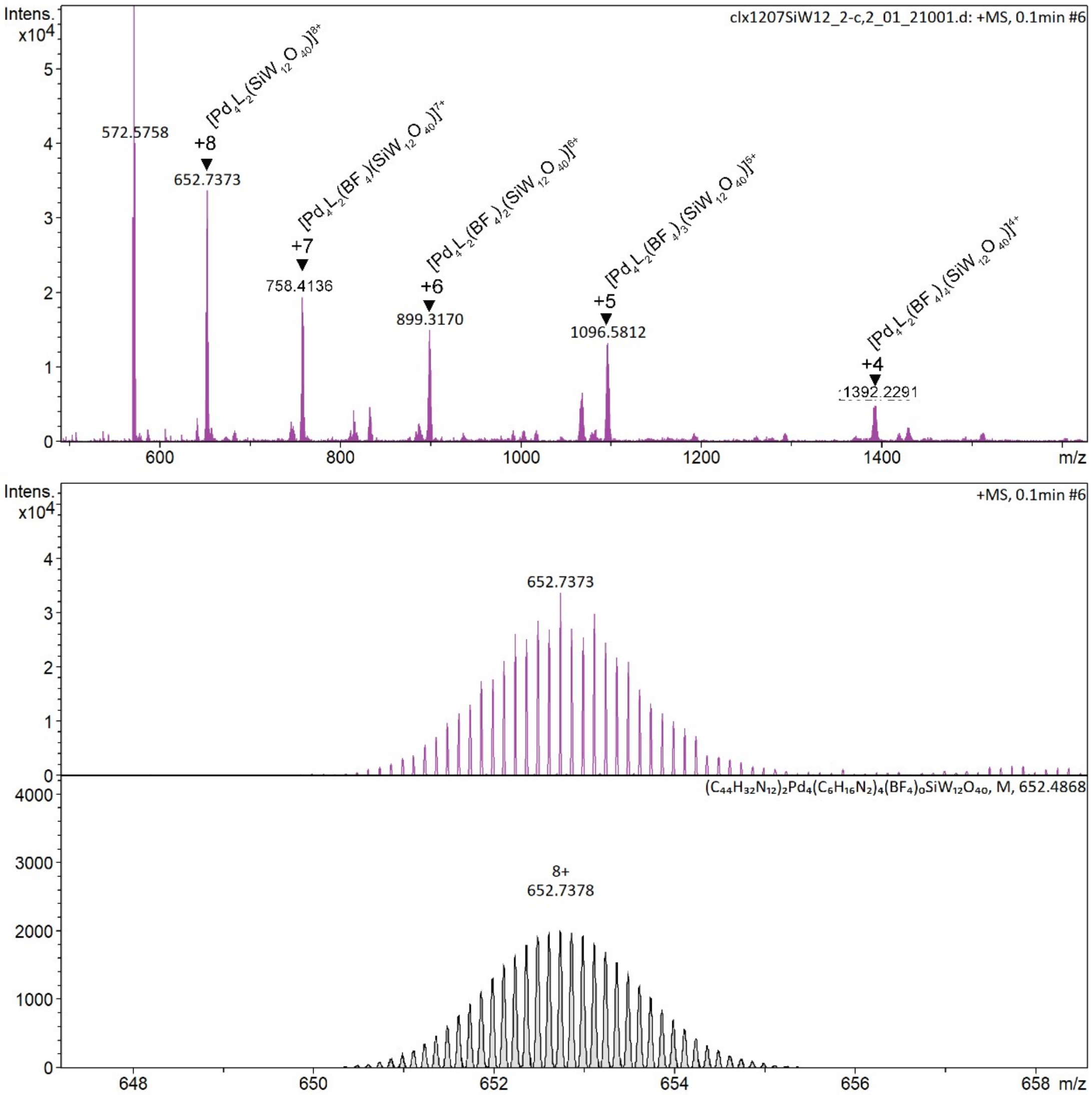

Figure S24. ESI-TOF-MS spectrum of the solution containing **1** with BF_4^- as the counterions and $SiW_{12}O_{40}^{4-}$, which is measured on an Impact II UHR-TOF mass spectrometry from Bruker.

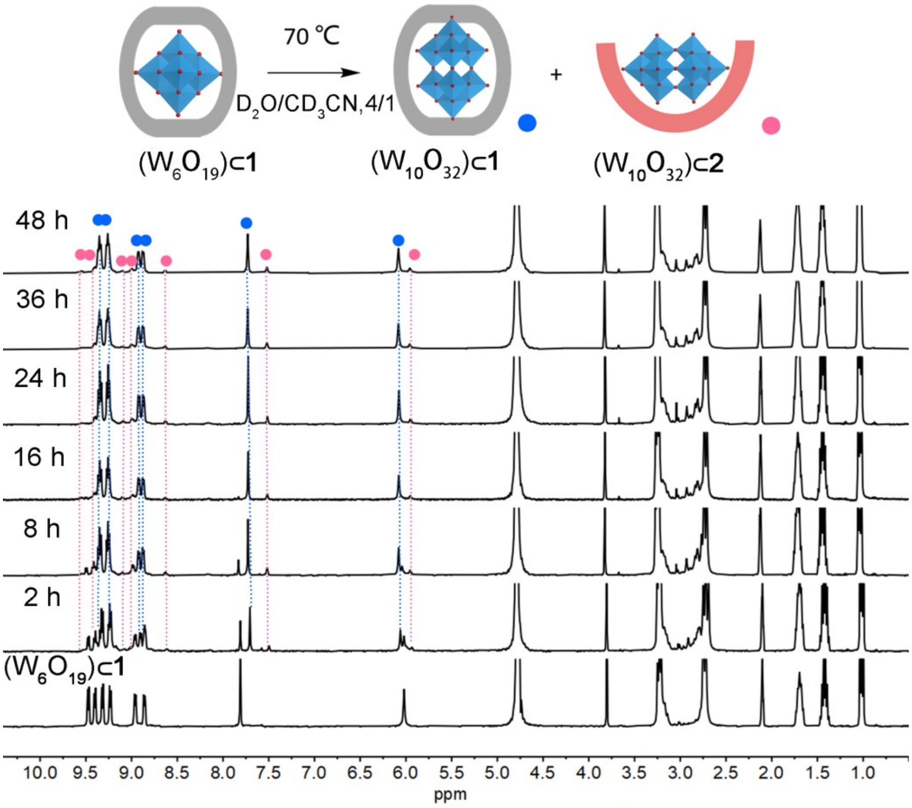

Figure S25. ^{1}H NMR change of **1**·$(NO_3)_{12}$ and 2 equiv. of $W_6O_{19}^{2-}$ with heating time at 70°C.

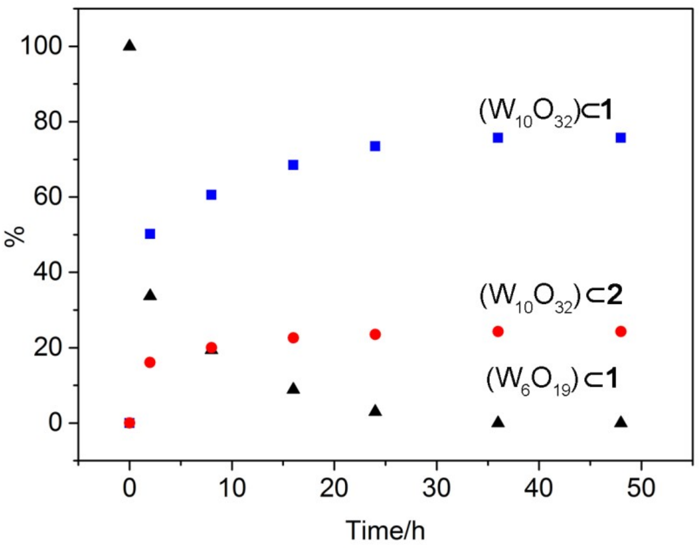

Figure S26. Distribution plots of host-guest complexes when heating the solution of **1**·$(NO_3)_{12}$ and 2 equiv. of $W_6O_{19}^{2-}$ at 70°C.

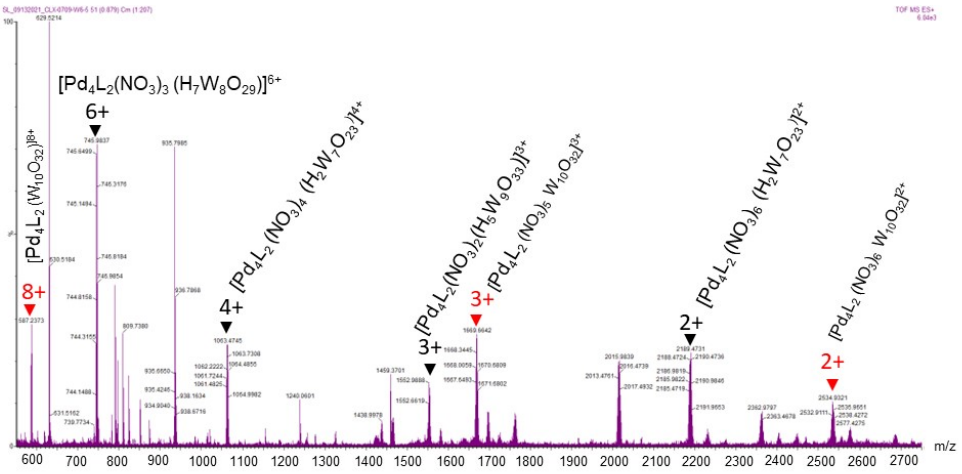

Figure S27. ESI-TOF-MS spectrum of the host-guest complex after heating the solution containing **1**·$(NO_3)_{12}$ and 2 equiv. of $W_6O_{19}^{2-}$ at 70°C for 48 h, which were recorded with a Waters Synapt G2 tandem mass spectrometer with traveling wave ion mobility separation capability.

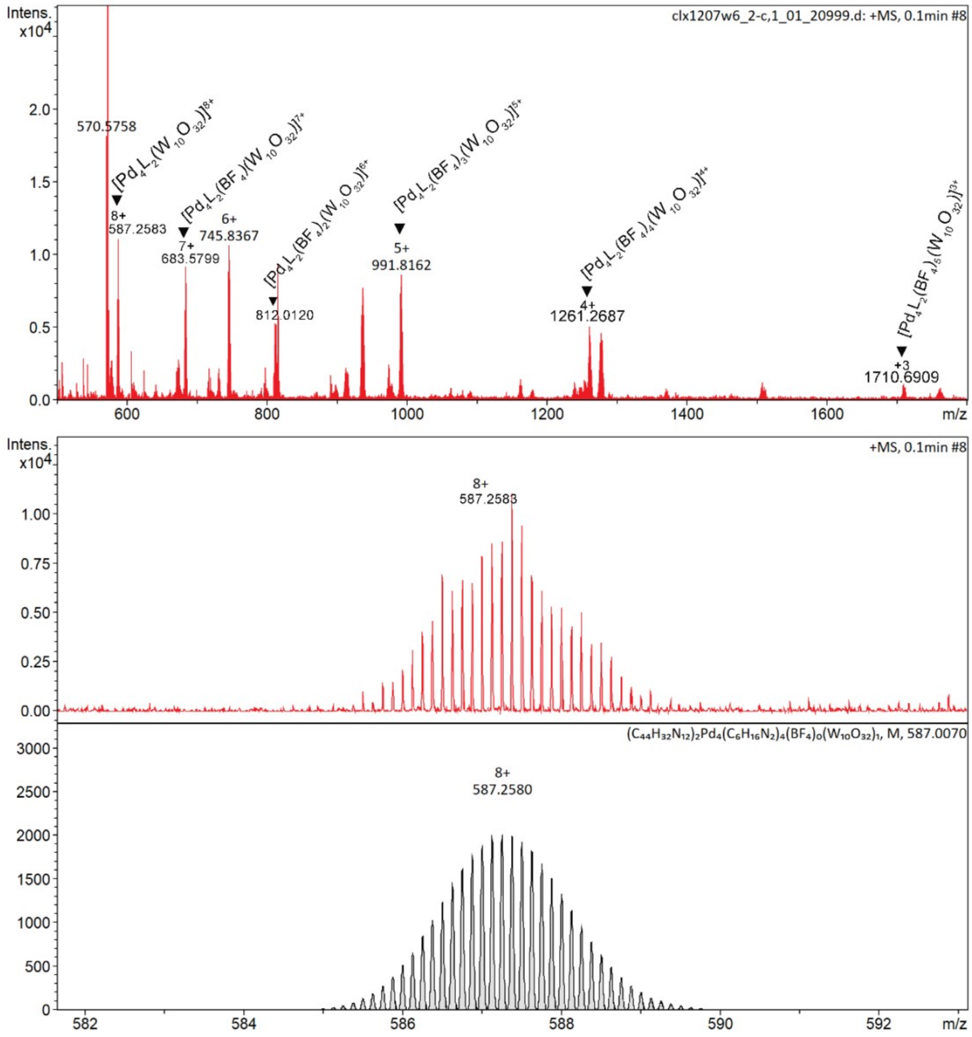

Figure S28. ESI-TOF-MS spectrum of the host-guest complex after heating the solution of containing **1** with BF_4^- salt and 2 equiv. of $W_6O_{19}^{2-}$, which is measured on an Impact II UHR-TOF mass spectrometry from Bruker.

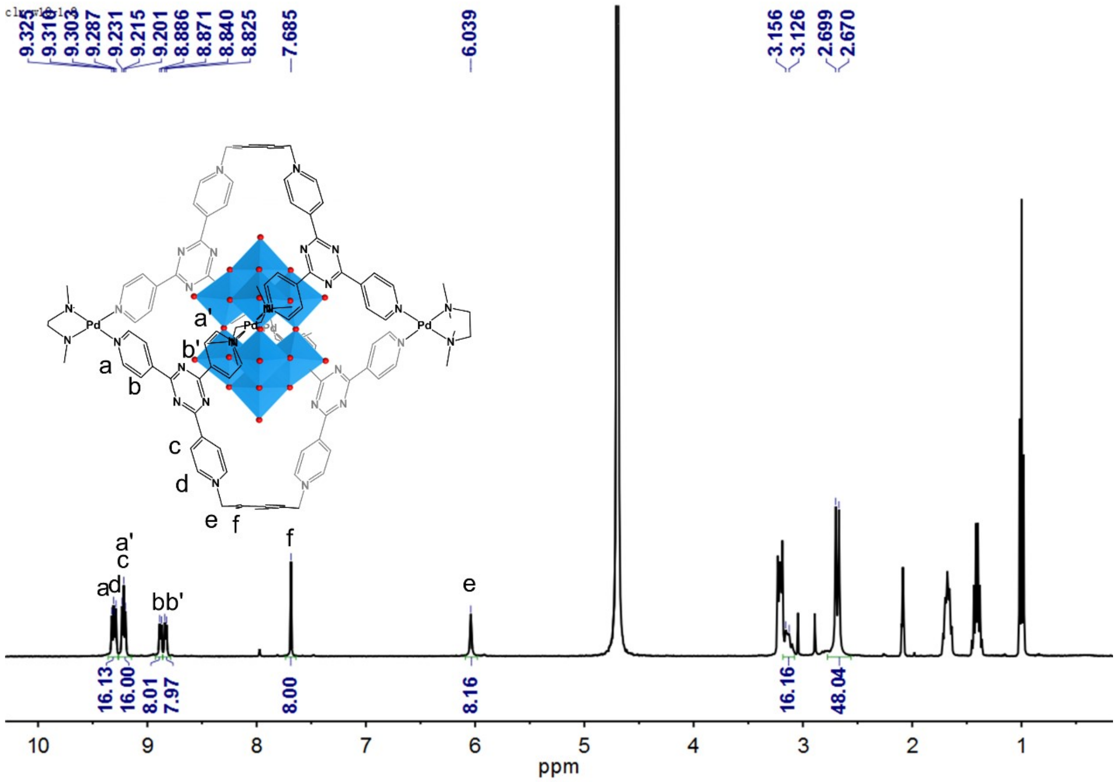

Figure S29. ^{1}H NMR spectrum of $(W_{10}O_{32})\subset\mathbf{1}\cdot(NO_3)_8$ (400 MHz, D_2O, 298 K).

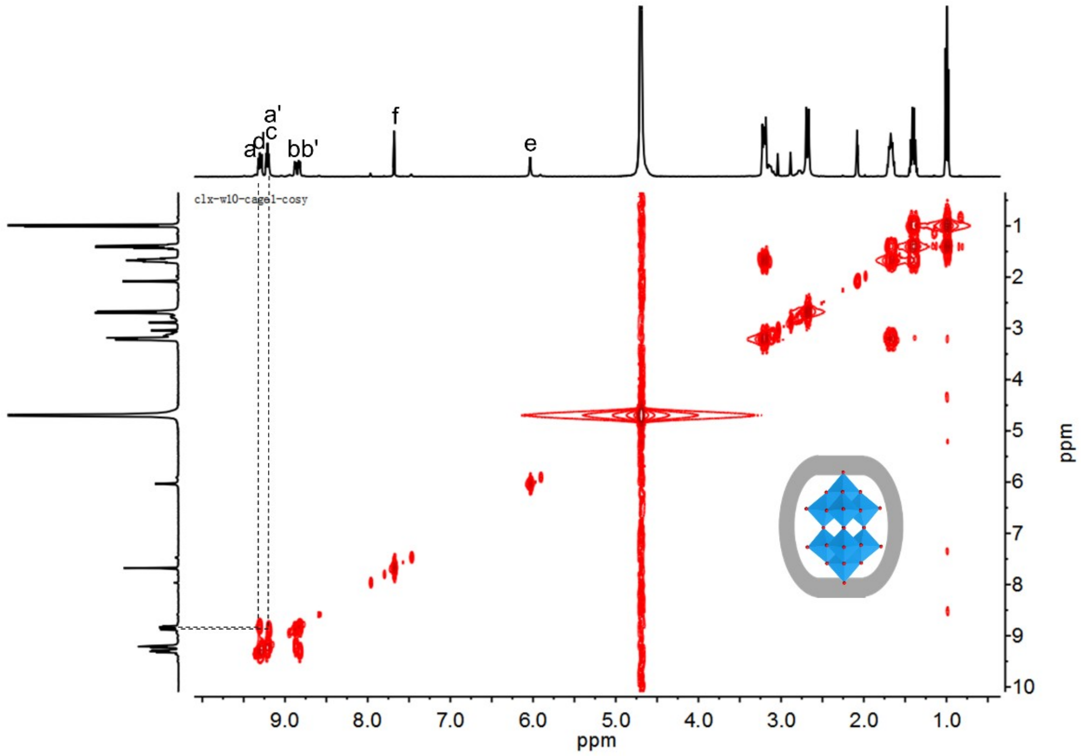

Figure S30. COSY NMR spectrum of $(W_{10}O_{32})\subset\mathbf{1}\cdot(NO_3)_8$ (400 MHz, D_2O, 298 K).

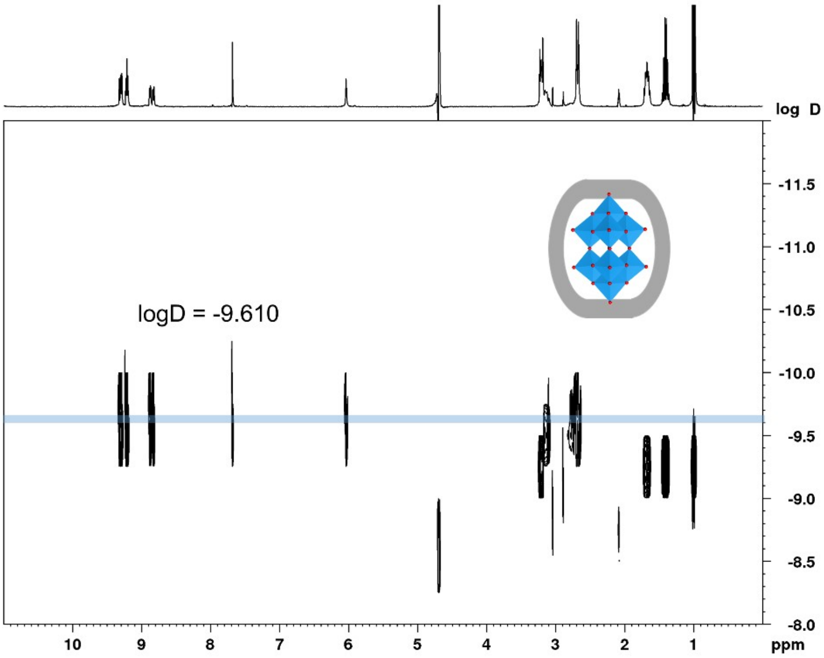

Figure S31. ^{1}H DOSY spectrum of $(W_{10}O_{32})\subset\mathbf{1}\cdot(NO_3)_8$ (400 MHz, D_2O, 298 K).

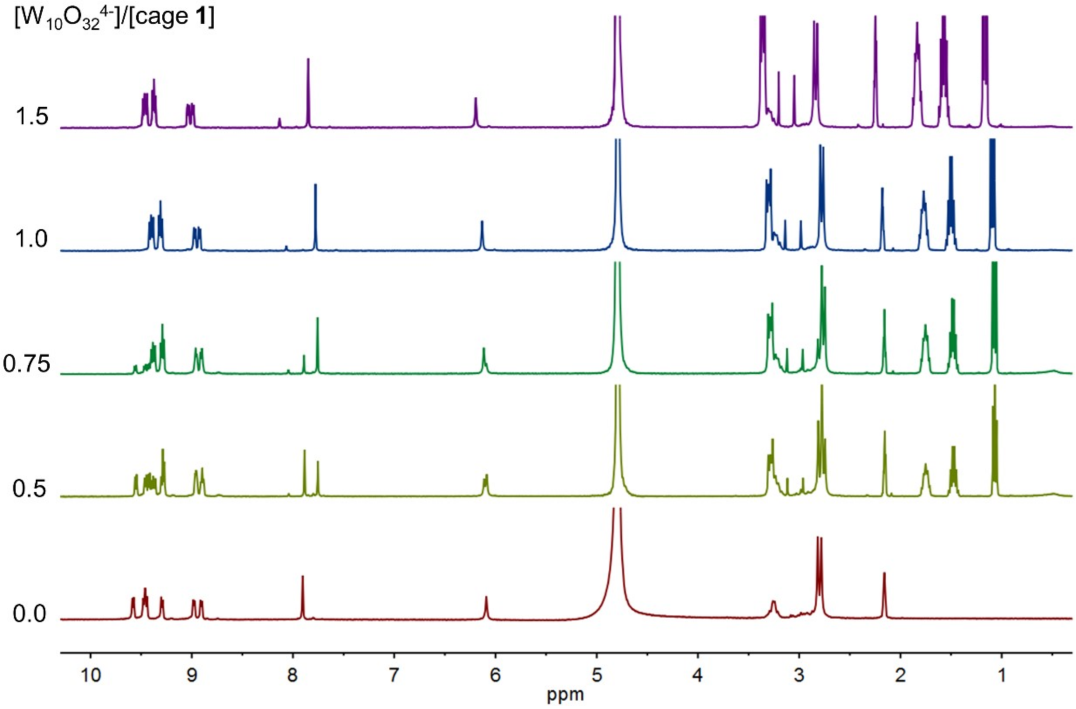

Figure S32. ^{1}H NMR spectra of a 1 mM solution of $\mathbf{1}\cdot(NO_3)_{12}$ in D_2O/CD_3CN (4/1) with 0-1.5 equiv of $W_{10}O_{32}^{4-}$ anion.

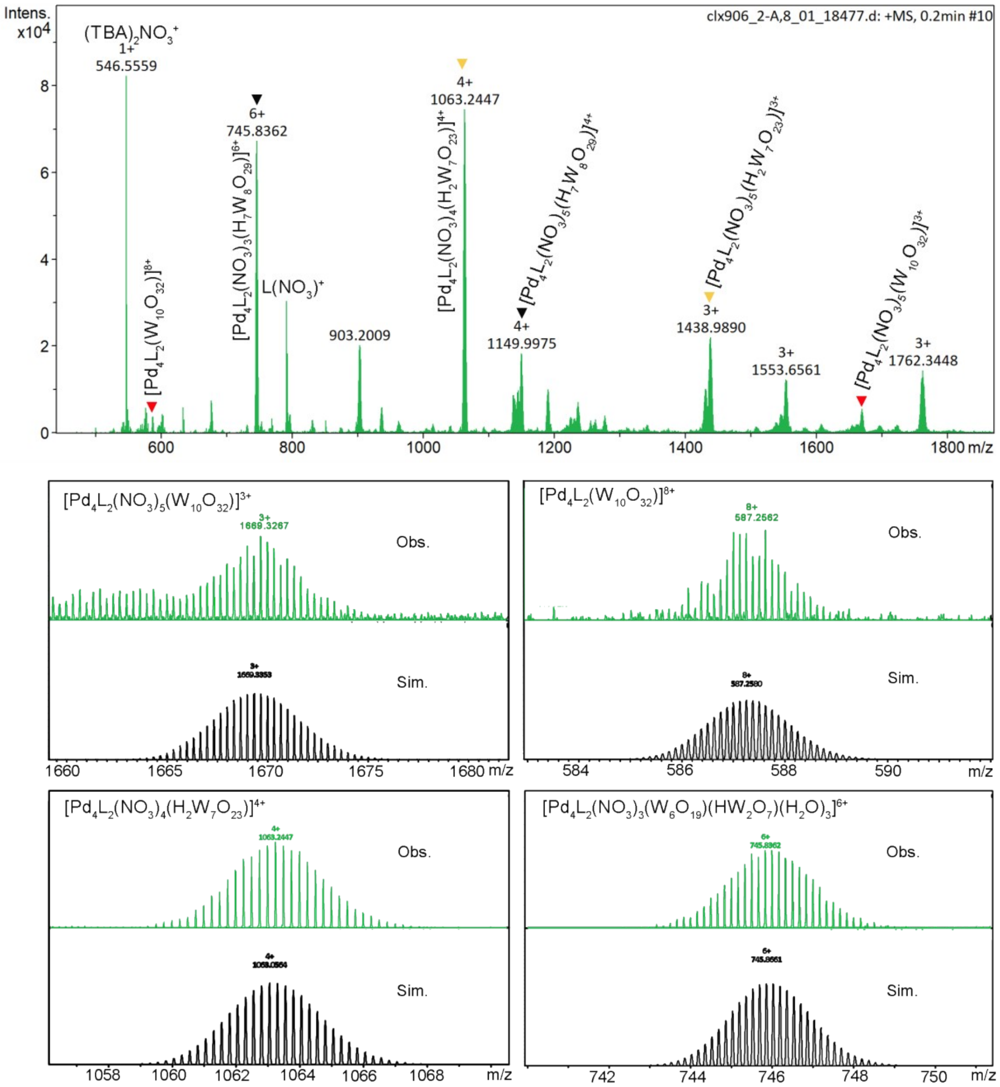

Figure S33. ESI-TOF-MS spectrum of $(W_{10}O_{32})\subset\mathbf{1}\cdot(NO_3)_8$, which is measured on an Impact II UHR-TOF mass spectrometry from Bruker.

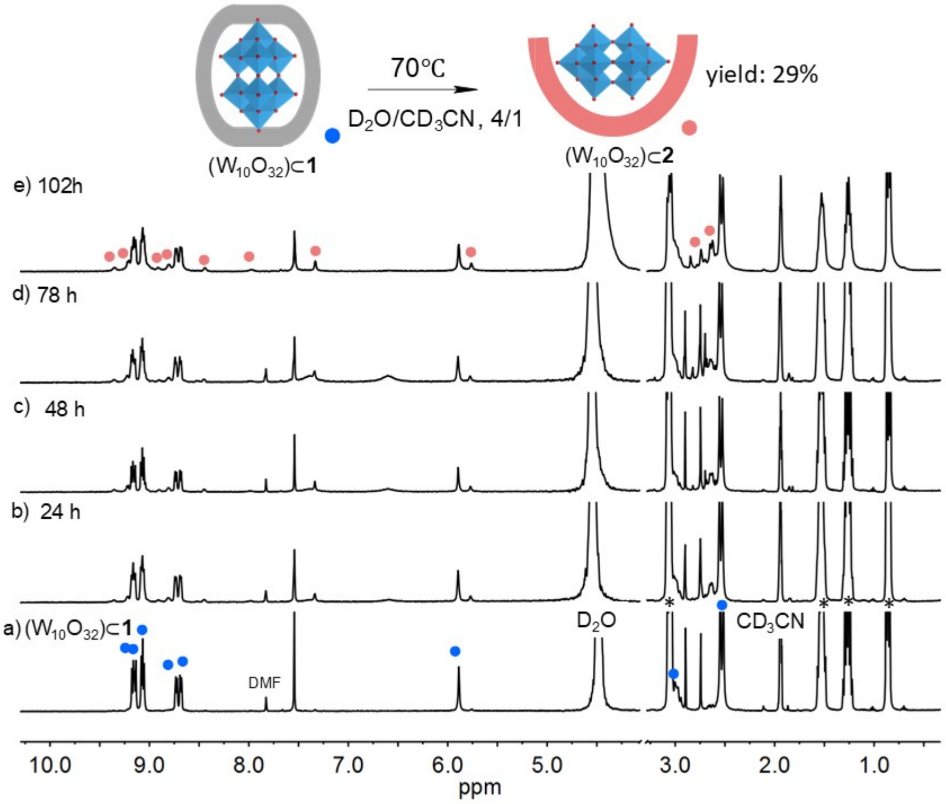

Figure S34. ^{1}H NMR change of $(W_{10}O_{32})\subset\mathbf{1}\cdot(NO_3)_8$ with heating time at 70°C (400 M, D_2O/CD_3CN 4/1, 298 K).

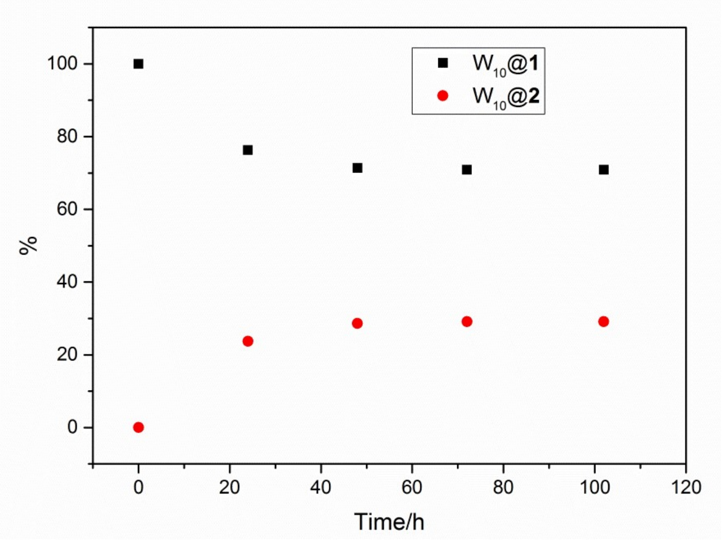

Figure S35. Distribution plots for the above cage-bowl transformation reaction.

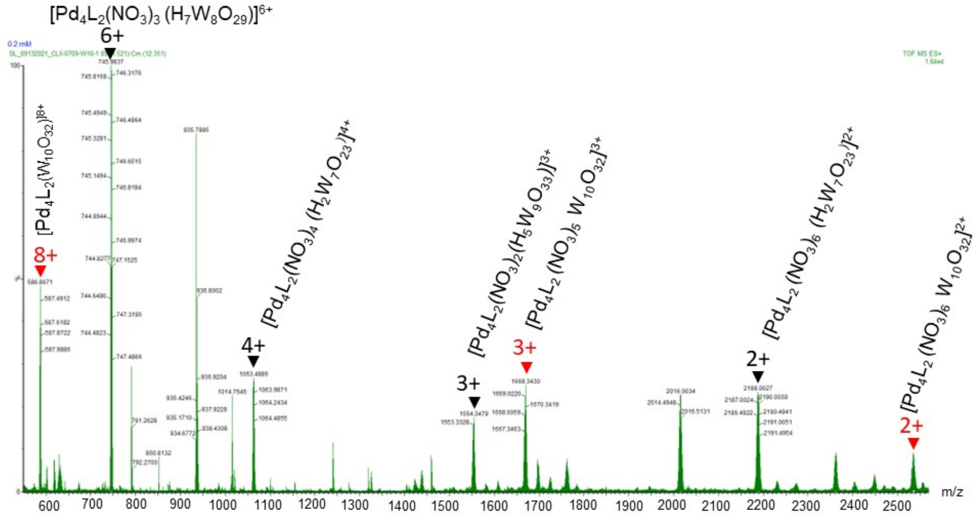

Figure S36. ESI-TOF-MS spectrum of $(W_{10}O_{32})\subset$**1**$\cdot(NO_3)_8$ aftering heating at 70°C, which were recorded with a Waters Synapt G2 tandem mass spectrometer with traveling wave ion mobility separation capability.

4. UV-Vis and IR spectra

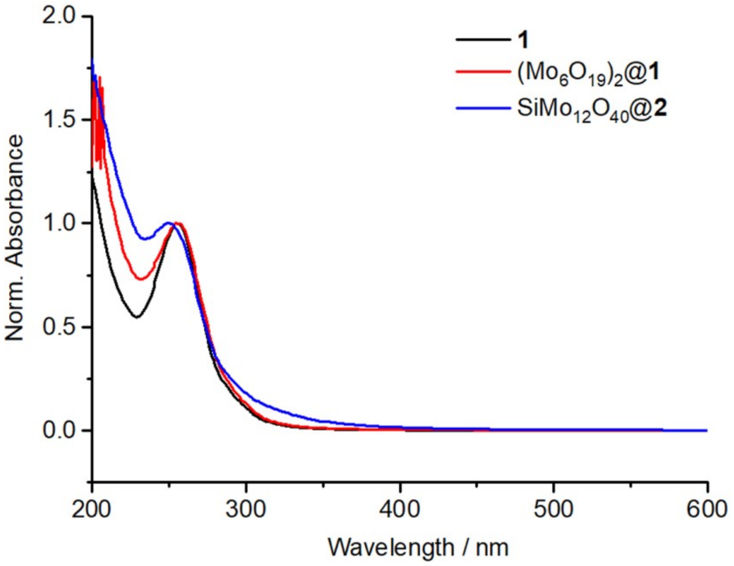

Figure S37. UV-Vis spectra of **1**$\cdot(NO_3)_{12}$, inclusion complex $(Mo_6O_{19})_2\subset$**1**$\cdot(NO_3)_8$, and $(SiMo_{12}O_{40})\subset$**2**$\cdot(NO_3)_8$ in H_2O.

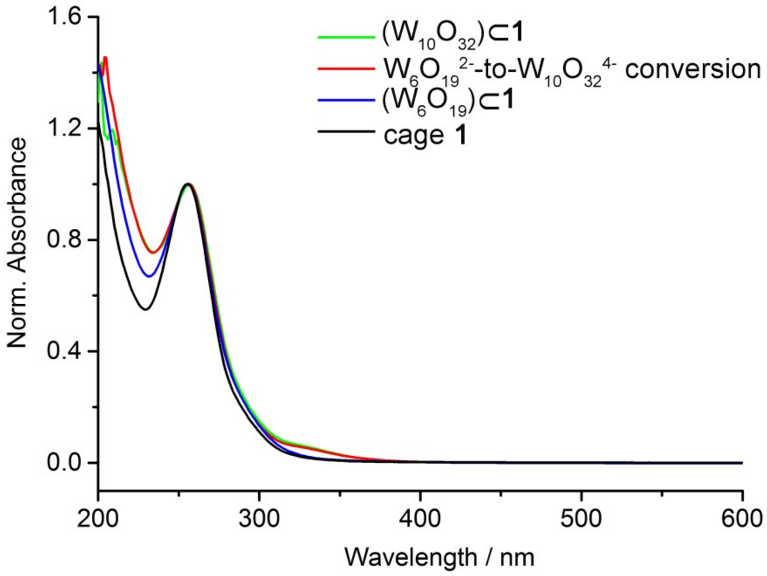

Figure S38. UV-Vis spectra of **1**·$(NO_3)_{12}$, inclusion complexes $(W_6O_{19})\subset$**1**·$(NO_3)_{10}$, and $(W_{10}O_{32})\subset$**1**·$(NO_3)_8$ in H_2O and the solution containing **1**·$(NO_3)_{12}$ and 2 equiv. of $W_6O_{19}^{2-}$ after heating at 70°C for 5 days.

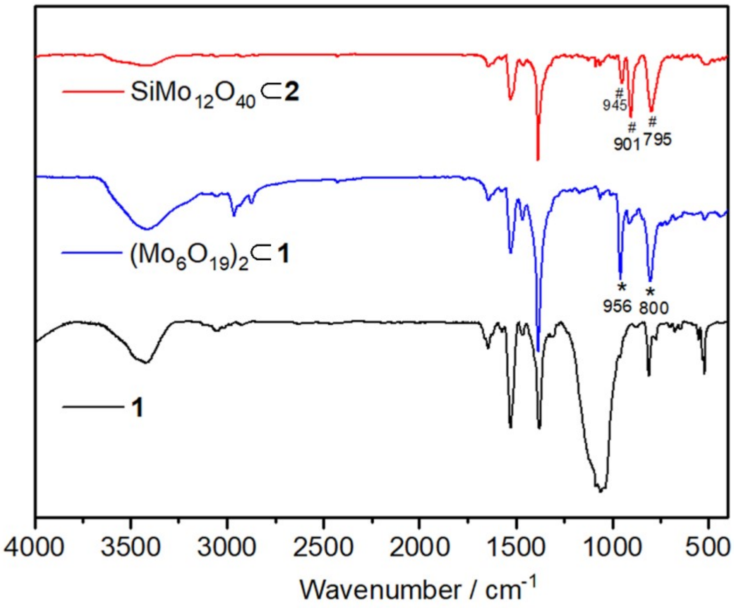

Figure S39. The IR spectra of **1**·$(NO_3)_{12}$, inclusion complexes $(Mo_6O_{19})_2 \subset$**1**·$(NO_3)_8$ and $(SiMo_{12}O_{40})\subset$**2**·$(NO_3)_8$ (crystal).

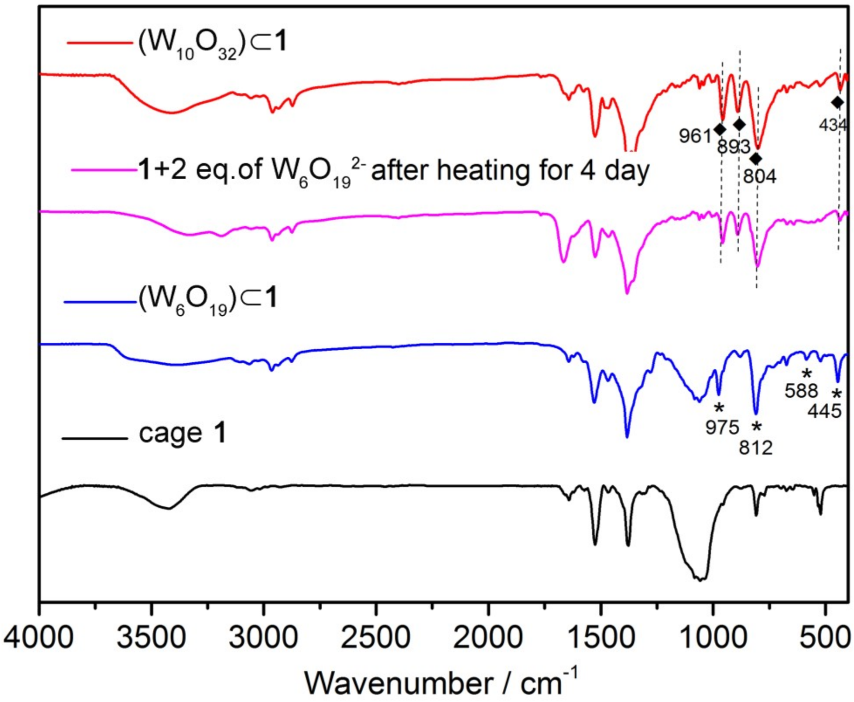

Figure S40. The IR spectra of **1**·$(NO_3)_{12}$, inclusion complexes (W_6O_{19})⊂**1**·$(NO_3)_{10}$ and $(W_{10}O_{32})$⊂**1**·$(NO_3)_8$, and the solid obtained from the solution of **1** and 2 equiv. of $W_6O_{19}^{2-}$ after heating for 4 days.

5. Control experiments and stability study

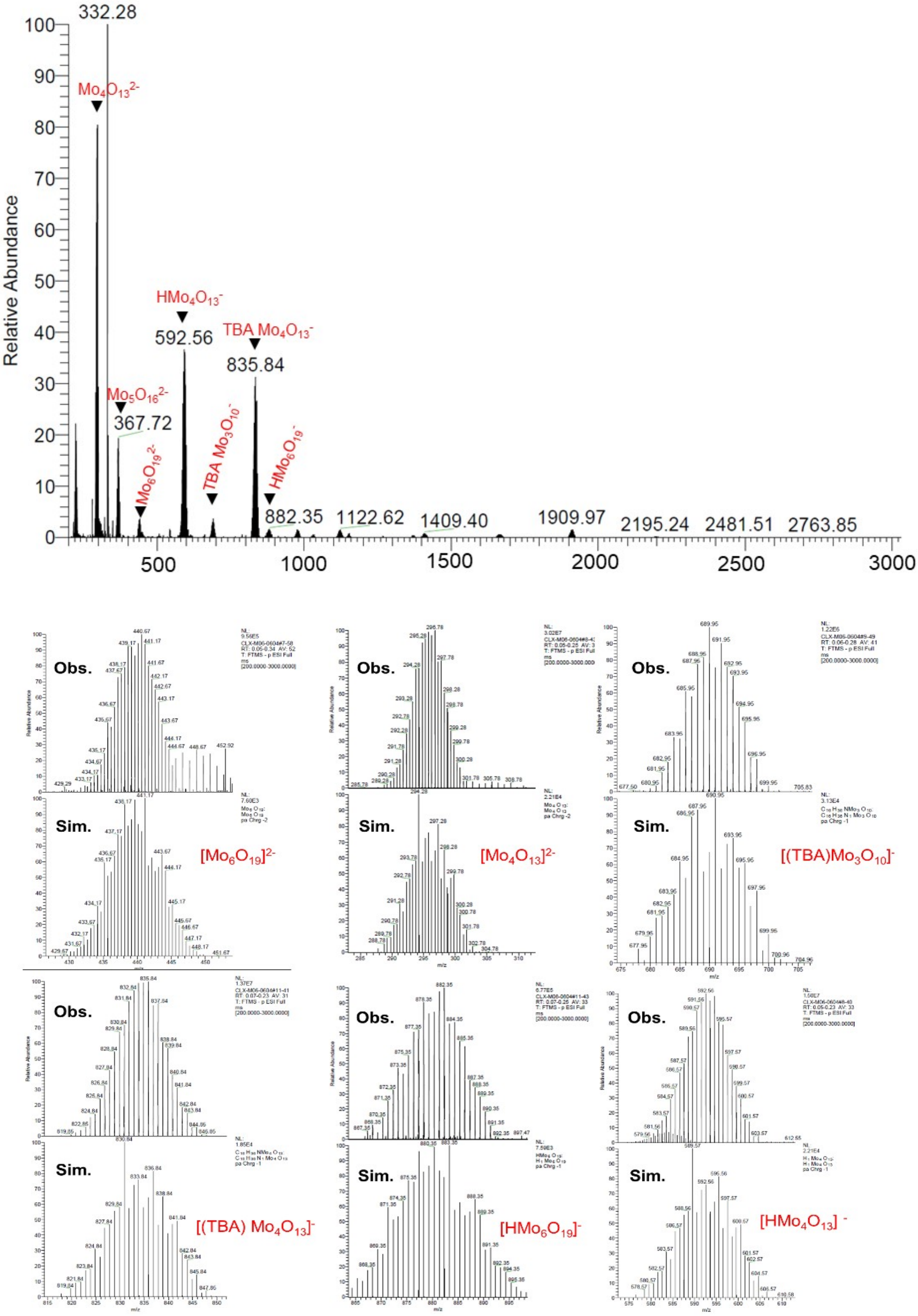

Figure S41. ESI-MS spectrum of $(TBA)_2Mo_6O_{19}$ and Na_2SiO_3 in a ratio of 1:1 after heating at 70°C for 4 days in water, measured on an Exactive Plus mass spectrometry from Thermo Fisher Scientific. As M_6O_{19} Lindqvist ion is known to be highly unstable in water, fragmented species, such as $Mo_3O_{10}^{2-}$ and $Mo_4O_{13}^{2-}$, due to the decomposition of $Mo_6O_{19}^{2-}$ ion were observed. No $SiMo_{12}O_{40}^{4-}$ ion was formed under this condition.

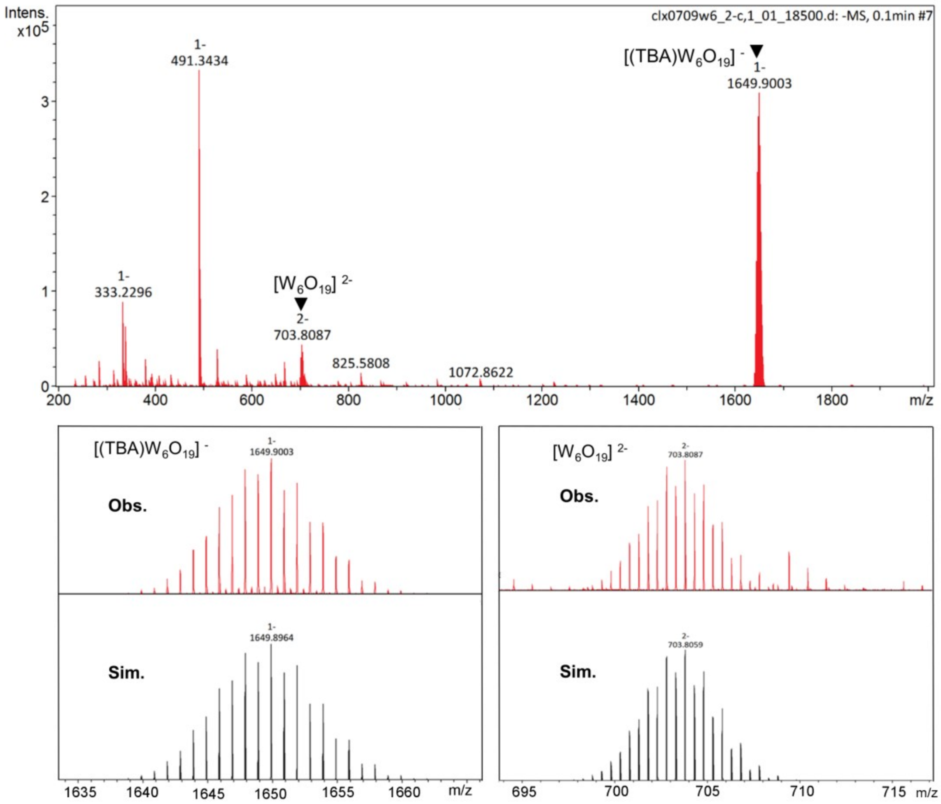

Figure S42. ESI-TOF-MS spectrum of $(TBA)_2W_6O_{19}$ and SiO_3^{2-} after heating at 70°C for 4 days in H_2O/CH_3CN(v/v, 4/1).

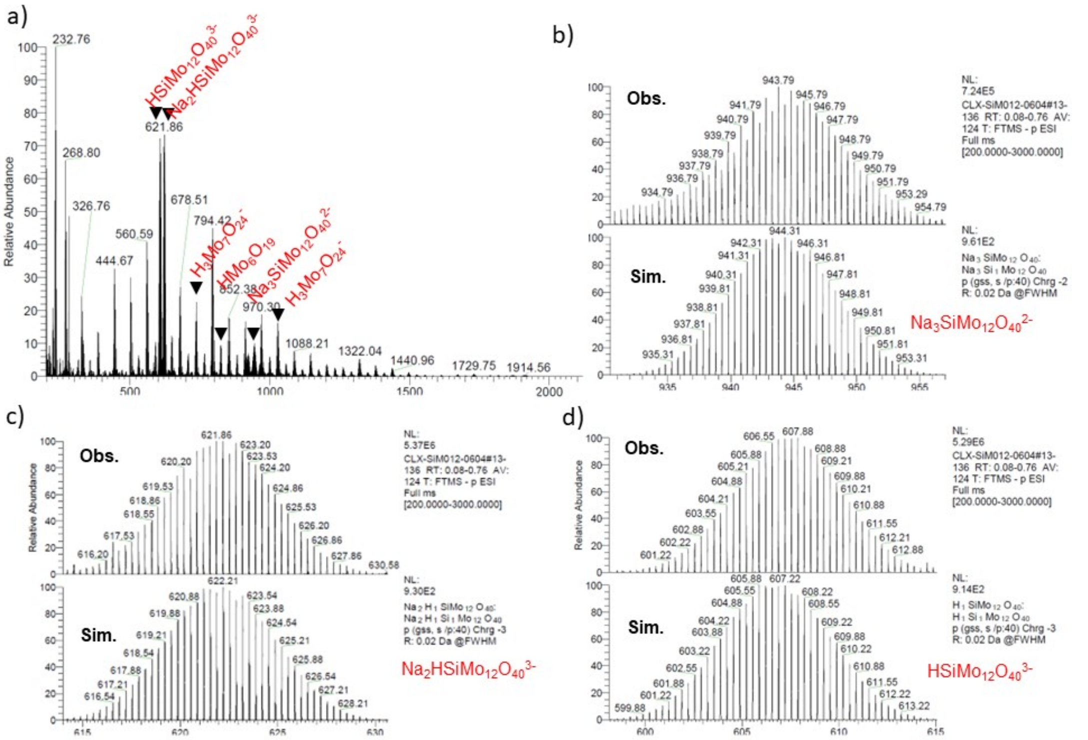

Figure S43. ESI-MS spectrum (a-d) of $H_4SiMo_{12}O_{40}$ after heating at 70°C for 4 days, measured on an Exactive Plus mass spectrometry from Thermo Fisher Scientific. Partial decomposition of $SiMo_{12}O_{40}^{4-}$ ion was observed.

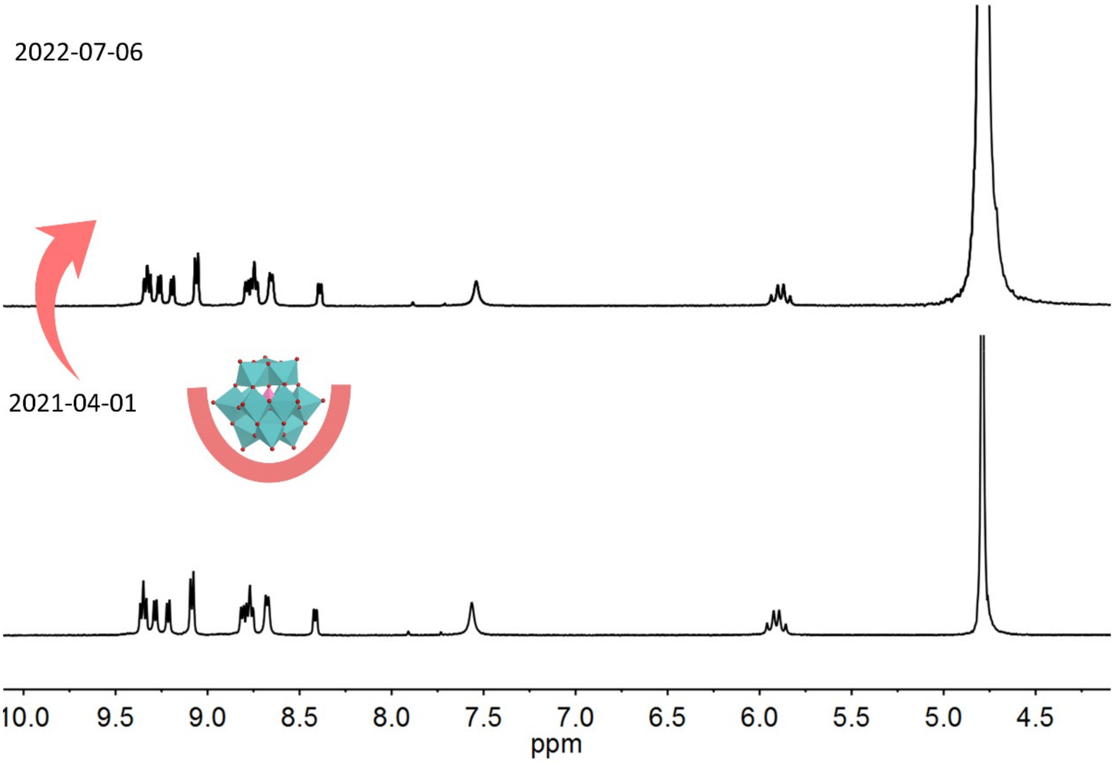

Figure S44. ^{1}H NMR change of the host-guest complex ($SiMo_{12}O_{40}$)⊂**2**·(NO_3)$_8$ after standing for 15 months at rt.

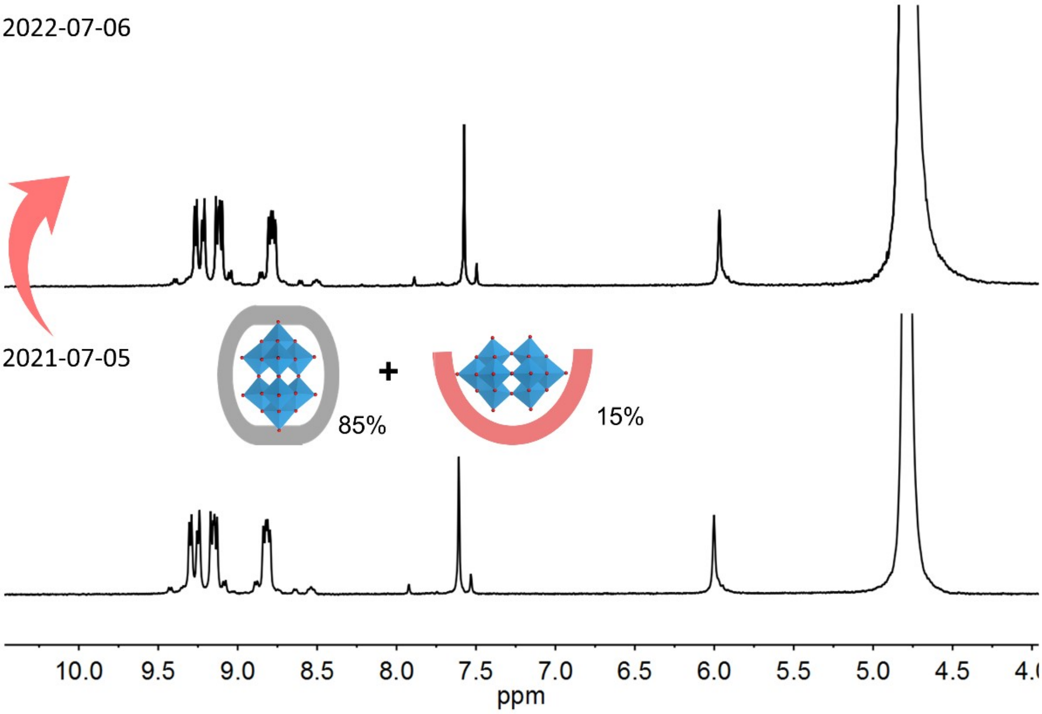

Figure S45. ^{1}H NMR change of the host-guest complexes ($W_{10}O_{32}$)⊂**1**·(NO_3)$_8$ and ($W_{10}O_{32}$)⊂**2**·(NO_3)$_8$ obtained from $W_6O_{19}^{2-}$ anion transformation after standing for 12 months at r.t.

6. Single crystal X - ray diffraction studies

Single crystal X-ray diffraction data for $(SiMo_{12}O_{40})\subset\mathbf{2}\cdot(NO_3)_8$ was performed on a Bruker D8 VENTURE photon II diffractometer with Iμs 3.0 microfocus X-ray source diffractometer. Data reduction was performed with the APEX-III software. X-ray diffraction study for $(W_{10}O_{32})\subset\mathbf{2}$ was carried out at the BL17B macromolecular crystallography beamline in SSRF. The collected diffraction data were processed with the HKL3000 software program. X-ray diffraction study for $(SiW_{12}O_{40})\subset\mathbf{2}$ was carried out on micro-focus metaljet diffractometer using Ga Kα radiation (λ = 1.3405 Å). Data reduction was performed with the CrysAlisPro package.[S3] These structures were solved by direct methods and refined by full-matrix least-squares on F^2 with anisotropic displacement using the SHELX software package.[S4] In all case, solvent molecules and some ions were highly disordered and could not be reasonably located. These residual intensities were removed by PLATON/SQUEEZE routine.[S5] PLATON/SQUEEZE routine was used to remove the contribution of the electron density associated with the remaining anions and highly disordered solvents. After accounting for the unresolved anions, the remaining masked electrons may correspond to the solvent molecules (H_2O) per Pd_4L_2 cage.

Crystal data for $(SiMo_{12}O_{40})\subset\mathbf{2}\cdot(NO_3)_8$: Space group $P6_3$, a = 55.438(3) Å, b = 55.438(3) Å, c = 34.467(2) Å, V = 91736(13) Å^3, Z = 18, T = 200(2) K. Anisotropic least - squares refinement for the framework atoms and isotropic refinement for the other atoms on 41961 independent merged reflections (R_{int}= 0.1551) converged at residual wR2 = 0.2746 for all data; residual R1 = 0.0935 for 27259 observed data [$I > 2\sigma(I)$], and goodness of fit (GOF) = 1.042. CCDC: 2360627.

Specific refinement details for $(SiMo_{12}O_{40})\subset\mathbf{2}$: Thermal parameter restraints (SIMU, DELU) were applied to obtain reasonable atomic displacement parameters. EADP was applied to constrain some atoms of tmenPd units and the ligand (located primarily at RESI LIG 1) to have identical anisotropic displacement parameters. Due to significant thermal motion within the structure, such as in the (tmen)Pd units, bond lengths and angles within the ions were restrained using SADI and DFIX. We also used the FLAT restriction command to maintain the planar tetragonal coordination mode of the Pd centers. The rigid group constraint AFIX 66 was also used to restrain the ring. We refined the host-guest complex in a chiral space group of *P*63 using a racemic-twinning model, because refinement in a higher symmetry space group of $P6_3m$ required a disorder modeling and gave less satisfactory results. We tried Platon's ADDSYM program to find the missing symmetry, but no higher symmetry was given.

Crystal data for $(W_{10}O_{32})\subset\mathbf{2}\cdot(NO_3)_8$: Space group $I4_1/a$, a = 57.774(8) Å, b = 57.774(8) Å, c = 36.483(7) Å, V = 121774(42) Å^3, Z = 16, T = 100(2) K. Anisotropic least - squares refinement for the framework atoms and decatungstate atoms and isotropic refinement for the other atoms on 31850 independent merged reflections (R_{int}= 0.09) converged at residual wR2 =0.2908 for all data; residual R1 = 0.0762 for 20094 observed data [$I > 2\sigma(I)$], and goodness of fit (GOF) = 1.060. (CCDC: 2380035)

Specific refinement details for $(W_{10}O_{32})\subset\mathbf{2}$: SIMU and DELU restraints were used to the whole framework and ions to obtain the chemical-reasonable models and reasonable atomic displacement parameters. RIGU restraint was used to one pyridyl ring of the ligand. DFIX Bond length restraint was used for some atoms of the ligands and tmenPd units. FLAT restraint was applied to nitrate ions. Some aromatic rings in the ligands were modelled as rigid groups using AFIX 66. Bond lengths and angles within tmenPd units were restrained to be similar to each other using SADI and SAME. OMIT restraint was used to delete three reflections with large Error/esd values.

Crystal data for $(SiW_{12}O_{40})\subset\mathbf{2}\cdot(NO_3)_8$: Space group $P2_1/n$, a = 33.1786(3) Å, b = 35.0845(4) Å, c = 58.0136(6) Å, V = 67530.9(15) Å^3, Z = 12, T = 293(2) K. Anisotropic least - squares refinement for the framework atoms and isotropic refinement for the other atoms on 39350 independent merged reflections (R_{int}= 0.0423) converged at residual wR2 = 0.3538 for all data; residual R1 = 0.1094 for 32799 observed data [$I > 2\sigma$ (I)], and goodness of fit (GOF) = 1.140. (CCDC: 2380036)

Specific refinement details for $(SiW_{12}O_{40})\subset\mathbf{2}\cdot(NO_3)_8$: Thermal parameter restraints (SIMU, DELU) were applied to the whole framework to obtain the chemical-reasonable models and reasonable atomic displacement parameters. Aromatic rings in the ligands were modelled as rigid groups using AFIX 66.

Note: One alert level A error and two alert level B errors were found through the IUCR's CheckCIF routine for the data of $(SiMo_{12}O_{40})\subset\mathbf{2}\cdot(NO_3)_8$. These alerts all result from the limited diffraction ability of this kind of giant supramolecular compounds in the crystal state. The crystal data quality is poor despite many attempts.

CheckCIF gives one alert level A and one alert level B error for $(W_{10}O_{32})\subset\mathbf{2}\cdot(NO_3)_8$. The crystals of this giant supramolecular host-guest complex diffract very weekly in nature, possibly due to a large amount of amorphous solvents and highly-disordered counterions existing in the unit cell. The resolution of the data is poor even when we collected the data on synchrotron beamlines. This is the best resolution that we have obtained after many optimizations based on synchrotron beamlines.

One A alert and one B alert are raised by the structure of $(SiW_{12}O_{40})\subset\mathbf{2}$. Some disordered frames, or amorphous solvents and highly disordered counter anions, result in a ratio of maximum / minimum residual density of 4.74. This does not affect the main conclusions.

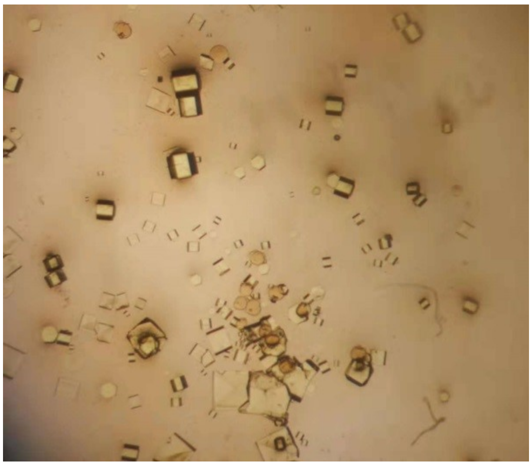

Figure S46. The crystals grown by slow evaporation of an aqueous solution of $(SiMo_{12}O_{40})\subset\mathbf{2}\cdot(NO_3)_8$.

IGM Calculations

Independent gradient model (IGM) analysis[S8] carried out with the Multiwfn 3.8 program[S9] was employed to investigate the intermolecular weak interactions and visualized with VMD 1.9.3 program.[S10] Strong polar attractions and van der Waals contacts are visualized as an iso-surface with blue and green colors, respectively. Single crystal structures were used as input files.

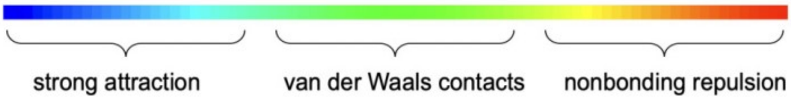

Figure S47. Color-coded sign $(\lambda_2)_\rho$ scale bar of IGM analysis.

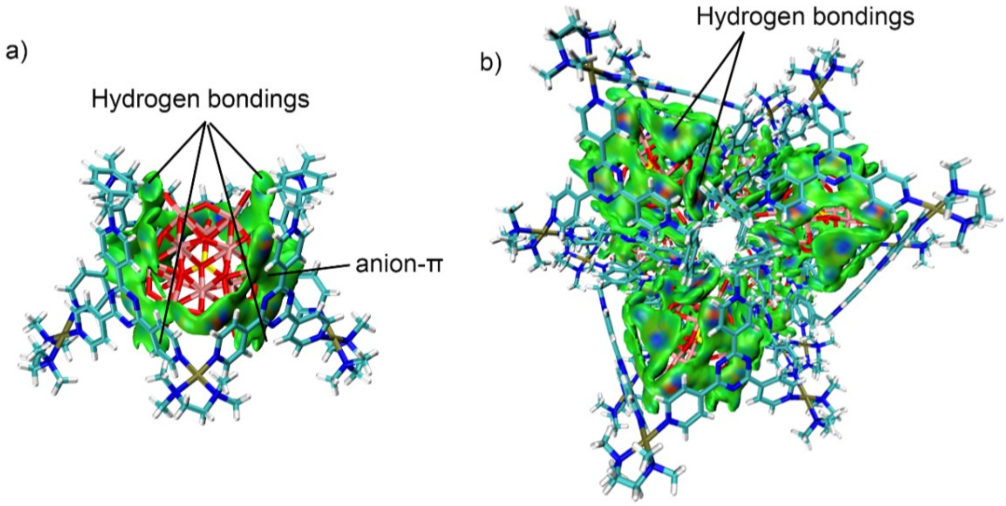

Figure S48.The capped-sticks representations of $(SiMo_{12}O_{40})\subset\mathbf{2}\cdot(NO_3)_8$ showing the intermolecular binding iso-surfaces between host and guest. $\delta_g^{inter}(\rho) = 0.003$ a.u. isosurface and all isosurfaces are colored according to a BGR (blue-green-red) scheme over the electron density range $-0.05 < \mathrm{sign}(\lambda_2)_\rho < 0.05$ a.u.

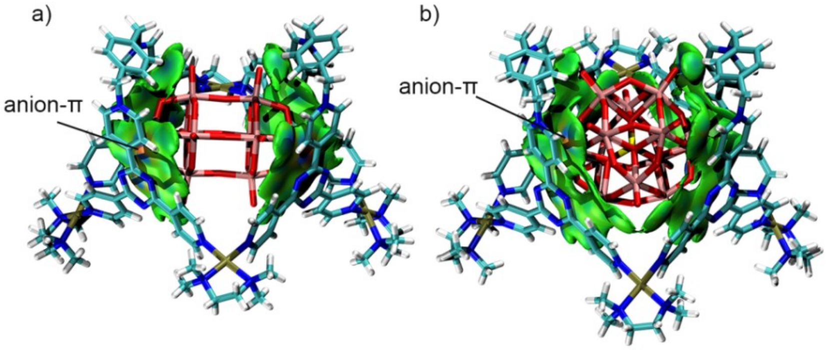

Figure S49.The capped-sticks representations of (a) $(W_{10}O_{40})\subset\mathbf{2}\cdot(NO_3)_8$ and (b) $(SiW_{12}O_{40})\subset\mathbf{2}\cdot(NO_3)_8$ showing the intermolecular binding iso-surfaces between host and guest. $\delta_g^{inter}(\rho) = 0.003$ a.u. isosurface and all isosurfaces are colored according to a BGR (blue-green-red) scheme over the electron density range $-0.05 < \mathrm{sign}(\lambda_2)_\rho < 0.05$ a.u.

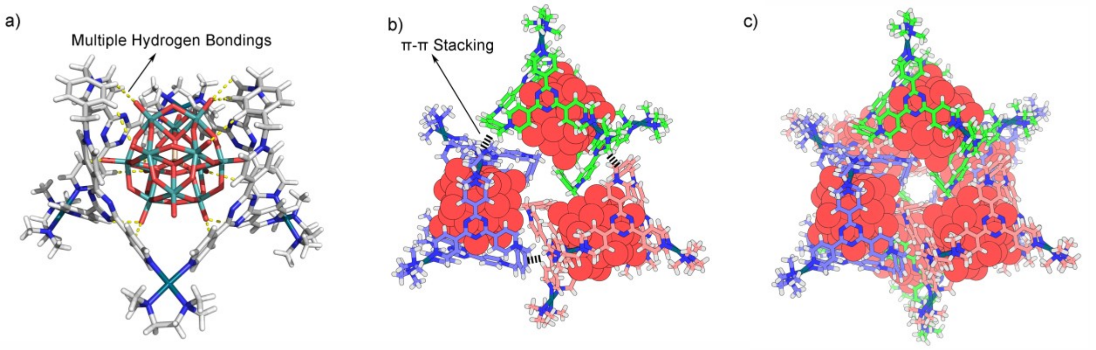

Figure S50. (a) Multiple hydrogen bondings of C-H···O=Mo in the structure of inclusion complex $(SiMo_{12}O_{40})\subset\mathbf{2}\cdot(NO_3)_8$. (b) The π-π interactions between p-xylene and TPT panels, with three host-guest complexes forming a trimer. (c) Crystal packing of the inclusion complex $(SiMo_{12}O_{40})\subset\mathbf{2}\cdot(NO_3)_8$.

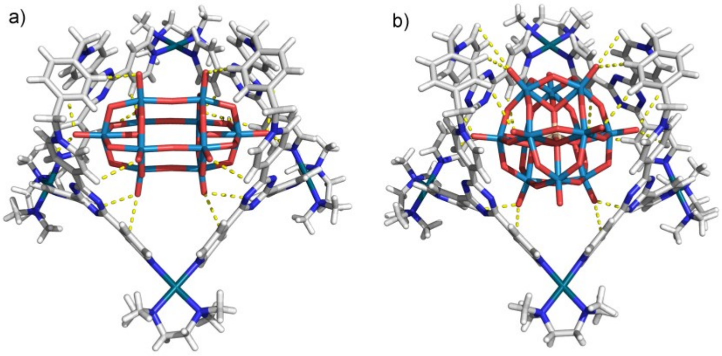

Figure S51. Multiple hydrogen bondings of C-H···O=Mo in the structure of inclusion complexes (a) $(W_{10}O_{32})\subset\mathbf{2}\cdot(NO_3)_8$ and (b) $(SiW_{12}O_{40})\subset\mathbf{2}\cdot(NO_3)_8$.

Cavity Volume Calculation

To determine the molecular volumes (V_{mol}) of the guest and the inner cavity volumes of the complexes, MoloVol calculations (https://molovol.com/)[S6] based on the crystal structures were performed using two-probe mode. The program parameters were set as follows: small probe radius: 1.2 Å; large probe radius: 6.0 Å; grid resolution: 0.2 Å; optimization depth: 4.

Table S1. Compiled data and percent volume occupancy.

POMs	V_{mol} (Å^3)	V_{bowl} (Å^3)	V_{cage} (Å^3)	Occupancy for bowl	Occupancy for cage
$SiMo_{12}O_{40}^{4-}$	658	963	914	68%	72.1%
$W_{10}O_{32}^{4-}$	558	968	914	58%	61%
$SiW_{12}O_{40}^{4-}$	669	970	914	71%	75%

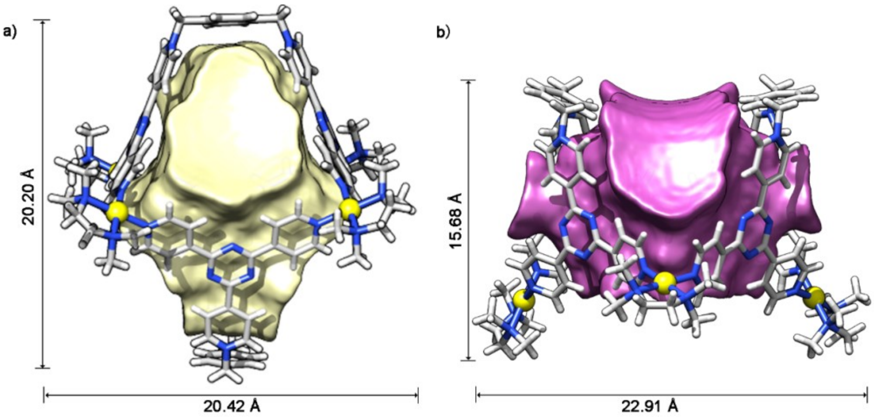

Figure S52. MoloVol-calculated cavity volumes of cage **1** and bowl **2**. The frameworks are represented as stick, and the cavity are shown as yellow surface. The cavity volumes of **1**, **2** was estimated as 914 Å^3 and 963 Å^3, respectively. Graphics were generated with UCSF Chimera. [S7]

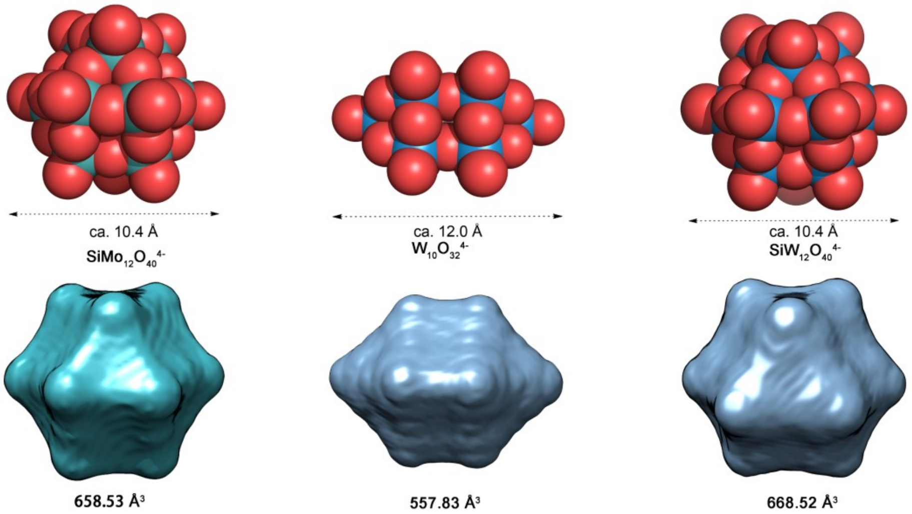

Figure S53. MoloVol-calculated Van der Waals volume of the anion guests $SiMo_{12}O_{40}^{4-}$, $W_{10}O_{32}^{2-}$, and $SiW_{12}O_{40}^{4-}$.

Table S2. Crystal data and structure refinement for ($SiMo_{12}O_{40}$)$\subset$**2**.

Identification code	p63_sq
Empirical formula	C112 H276 Mo12 N40 O138 Pd4 Si
Formula weight	5996.68
Temperature	200(2) K
Wavelength	0.71073 Å
Crystal system	Hexagonal
Space group	$P6_3$
Unit cell dimensions	a = 55.438(4) Å α= 90°.
	b = 55.438(4) Å β= 90°.
	c = 34.467(2) Å γ = 120°.
Volume	91736(13) $Å^3$
Z	18
Density (calculated)	1.954 Mg/m^3
Absorption coefficient	1.187 mm^{-1}
F(000)	54612
Crystal size	0.15 x 0.13 x 0.10 mm^3
Theta range for data collection	2.182 to 17.999°.
Index ranges	-48<=h<=48, -48<=k<=46, -29<=l<=29
Reflections collected	284618
Independent reflections	41961 [R(int) = 0.1551]
Completeness to theta = 17.999°	99.7 %
Absorption correction	Semi-empirical from equivalents
Max. and min. transmission	0.7446 and 0.5834
Refinement method	Full-matrix least-squares on F^2
Data / restraints / parameters	41961 / 11885 / 4608
Goodness-of-fit on F^2	1.042
Final R indices [I>2sigma(I)]	R1 = 0.0935, wR2 = 0.2345
R indices (all data)	R1 = 0.1389, wR2 = 0.2746
Absolute structure parameter	0.57(8)
Extinction coefficient	n/a
Largest diff. peak and hole	2.333 and -1.156 e.$Å^{-3}$

Table S3. Crystal data and structure refinement for $(W_{10}O_{32})\subset$**2**.

Identification code	output_sq_s
Empirical formula	C112 H319 N40 O151.50 Pd4 W10
Formula weight	6915.15
Temperature	100(2) K
Wavelength	0.68875 Å
Crystal system	Tetragonal
Space group	$I4_1/a$
Unit cell dimensions	a = 57.774(8) Å α= 90°.
	b = 57.774(8) Å β= 90°.
	c = 36.483(7) Å γ = 90°.
Volume	121774(42) Å^3
Z	16
Density (calculated)	1.509 Mg/m^3
Absorption coefficient	3.736 mm^{-1}
F(000)	54512
Crystal size	0.12 x 0.10 x 0.08 mm^3
Theta range for data collection	0.966 to 20.142°.
Index ranges	0<=h<=67, -42<=k<=42, 0<=l<=42
Reflections collected	31850
Independent reflections	31850 [R(int) = 0.09]
Completeness to theta = 20.142°	99.9 %
Absorption correction	Semi-empirical from equivalents
Max. and min. transmission	0.7444 and 0.4396
Refinement method	Full-matrix least-squares on F^2
Data / restraints / parameters	31850 / 1917 / 1643
Goodness-of-fit on F^2	1.060
Final R indices [I>2sigma(I)]	R1 = 0.0762, wR2 = 0.2604
R indices (all data)	R1 = 0.1046, wR2 = 0.2908
Extinction coefficient	n/a
Largest diff. peak and hole	1.506 and -0.839 e.Å^{-3}

Table S4. Crystal data and structure refinement for $(SiW_{12}O_{40})\subset\mathbf{2}$.

Identification code	p21n-a_sq_s
Empirical formula	C112 H228 N40 O114 Pd4 Si W12
Formula weight	6619.22
Temperature	293(2) K
Wavelength	1.34139 Å
Crystal system	Monoclinic
Space group	$P2_1/n$
Unit cell dimensions	a = 33.1786(3) Å α= 90°.
	b = 35.0845(4) Å β= 89.8996(10)°.
	c = 58.0136(6) Å γ = 90°.
Volume	67530.9(11) $Å^3$
Z	12
Density (calculated)	1.953 Mg/m^3
Absorption coefficient	9.843 mm^{-1}
F(000)	38136
Crystal size	0.25 x 0.13 x 0.10 mm^3
Theta range for data collection	2.072 to 33.980°.
Index ranges	-25<=h<=27, -29<=k<=18, -48<=l<=29
Reflections collected	96650
Independent reflections	39350 [R(int) = 0.0423]
Completeness to theta = 33.980°	96.1 %
Absorption correction	Gaussian
Max. and min. transmission	0.921 and 0.384
Refinement method	Full-matrix-block least-squares on F^2
Data / restraints / parameters	39350 / 6195 / 4877
Goodness-of-fit on F^2	1.140
Final R indices [I>2sigma(I)]	R1 = 0.1094, wR2 = 0.3409
R indices (all data)	R1 = 0.1168, wR2 = 0.3538
Extinction coefficient	n/a
Largest diff. peak and hole	6.718 and -1.417 e.$Å^{-3}$

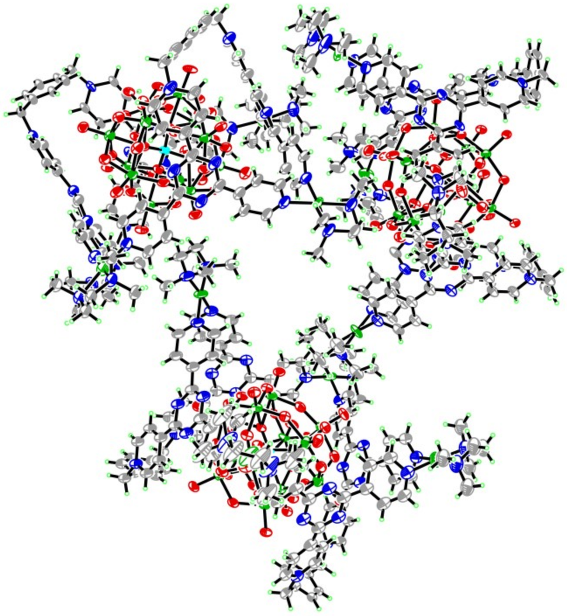

Figure S54. Ortep drawing of the asymmetric unit in the crystal structure of the inclusion complex $(SiMo_{12}O_{40})\subset\mathbf{2}\cdot(NO_3)_8$ at 30% probability level.

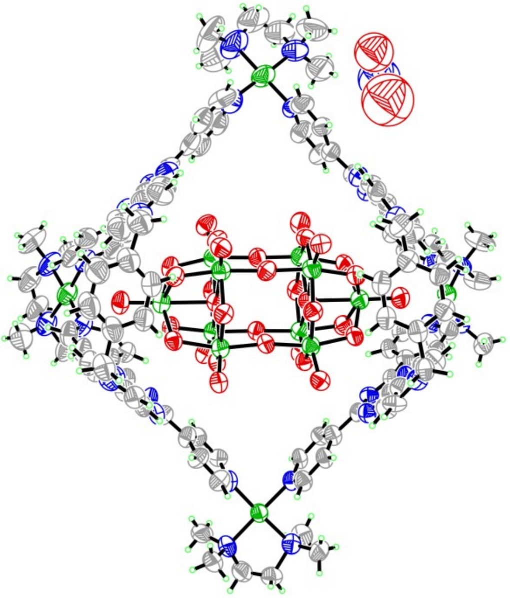

Figure S55. Ortep drawing of the asymmetric unit in the crystal structure of the inclusion complex $(W_{10}O_{32})\subset\mathbf{2}\cdot(NO_3)_8$ at 30% probability level.

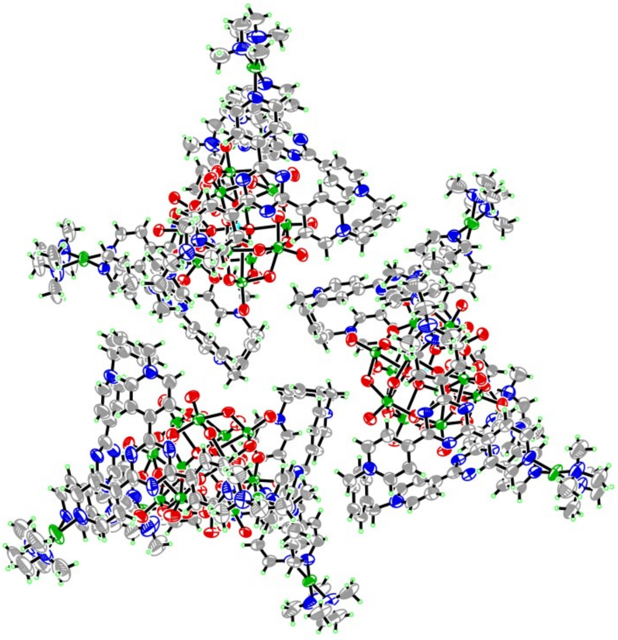

Figure S56. Ortep drawing of the asymmetric unit in the crystal structure of the inclusion complex $(SiW_{12}O_{40})\subset\mathbf{2}\cdot(NO_3)_8$ at 30% probability level.

7. Reference

S1. Li, S.-C.; Cai, L.-X.; Zhou, L.-P.; Guo, F.; Sun, Q.-F. *Sci. China Chem.* **2019**, *62* (6), 713-718.

S2. Cai, L. X.; Li, S. C.; Yan, D. N.; Zhou, L. P.; Guo, F.; Sun, Q. F. *J. Am. Chem. Soc.* **2018**, *140*, 4869-4876.

S3. Agilent Technologies, CrysAlisPro v. 1.171.36.28, 2013.

S4. Sheldrick, G. M. *Acta Crystallogr. Sect. A*, **2008**, *64*, 112-122.

S5. Spek, A. L. *J. Appl. Crystallogr.* **2003**, *36*, 7-13.

*S*6. Maglic, J. B.; Lavendomme, R. *J. Appl. Crystallogr.* **2022**, *55*, 1033-1044.

S7. Pettersen, E. F.; Goddard, T. D.; Huang, C. C.; Couch, G. S.; Greenblatt, D. M.; Meng E. C.; Ferrin, T. E. *J. Comput. Chem.* **2004**, 1605-1612.

S8. Lefebvre, C.; Rubez, G.; Khartabil, H.; Boisson, J.-C.; Contreras-García, J.; Hénon, E. *Phys. Chem. Chem. Phys.* **2017**, *19*, 17928-17936.

S9. Lu, T.; Chen, F. *J. Comput. Chem.* **2012**, *33*, 580-592.

S10. Humphrey, W.; Dalke, A.; Schulten, K. *J. Mol. Graphics.* **1996**, *14*, 33-38.